UNITED NATIONS UNIVERSITY
GEOTHERMAL TRAINING PROGRAMME
Orkustofnun, Grensásvegur 9,
IS-108 Reykjavík, Iceland

Reports 2009
Number 4

CARBON DIOXIDE FIXATION BY CALCITE AND DIFFUSIVE DEGASSING IN THE SOUTHERN REGION OF THE BERLÍN GEOTHERMAL SYSTEM, EL SALVADOR

MSc thesis
Department of Earth Sciences
University of Iceland

by

Roberto Enrique Renderos
LaGeo S.A. de C.V.
15 Av. Sur, Colonia Utila
Santa Tecla, La Libertad
EL SALVADOR

United Nations University
Geothermal Training Programme
Reykjavík, Iceland
Published in December 2009

ISBN 978-9979-68-269-1
ISSN 1670-7427

This MSc thesis has also been published in June 2009 by the
Faculty of Science – Department of Earth Sciences
University of Iceland

INTRODUCTION

The Geothermal Training Programme of the United Nations University (UNU) has operated in Iceland since 1979 with six month annual courses for professionals from developing countries. The aim is to assist developing countries with significant geothermal potential to build up groups of specialists that cover most aspects of geothermal exploration and development. During 1979-2009, 424 scientists and engineers from 44 countries have completed the six month courses. They have come from Asia (43%), Africa (28%), Central America (15%), and Central and Eastern Europe (14%). There is a steady flow of requests from all over the world for the six month training and we can only meet a portion of the requests. Most of the trainees are awarded UNU Fellowships financed by the UNU and the Government of Iceland.

Candidates for the six month specialized training must have at least a BSc degree and a minimum of one year practical experience in geothermal work in their home countries prior to the training. Many of our trainees have already completed their MSc or PhD degrees when they come to Iceland, but several excellent students who have only BSc degrees have made requests to come again to Iceland for a higher academic degree. In 1999, it was decided to start admitting UNU Fellows to continue their studies and study for MSc degrees in geothermal science or engineering in co-operation with the University of Iceland. An agreement to this effect was signed with the University of Iceland. The six month studies at the UNU Geothermal Training Programme form a part of the graduate programme.

It is a pleasure to introduce the twentieth UNU Fellow to complete the MSc studies at the University of Iceland under the co-operation agreement. Mr. Roberto Enrique Renderos, BEng. in Industrial Engineering, from PT. Pertamina Geothermal Energy, completed the six month specialized training in Geothermal Utilization at the UNU Geothermal Training Programme in October 2002. His research report was entitled "Chemical characterization of the thermal fluid discharge from well production tests in the Berlín geothermal field, El Salvador". After five years of geothermal research work in El Salvador, he came back to Iceland for MSc studies at the Faculty of Science – Department of Earth Sciences of the University of Iceland in September 2007. In June 2009, he defended his MSc thesis presented here, entitled "Carbon dioxide fixation by calcite and diffusive degassing in the southern region of the Berlín geothermal system, El Salvador". His studies in Iceland were financed by a fellowship from the Government of Iceland through the UNU Geothermal Training Programme. Roberto is the first Salvadorian to complete his MSc studies on a fellowship from UNU-GTP. We congratulate him on his achievements and wish him all the best for the future. We thank the Faculty of Science of the University of Iceland for the co-operation, and his supervisors for the dedication.

Finally, I would like to mention that Roberto's MSc thesis with the figures in colour is available for downloading on our website at page *www.unugtp.is/publications.*

With warmest wishes from Iceland,

Ingvar B. Fridleifsson, director
United Nations University
Geothermal Training Programme

ACKNOWLEDGEMENT

I would like to express my gratitude to The Government of Iceland, through the United Nations University Geothermal Training Programme (UNU-GTP), for funding this Master of Science studies; and to Lageo S.A. de C.V. for officially supporting my studies in Iceland.

I extend my gratitude to my supervisor Dr. Halldór Ármannsson for his patience, support and guidance to complete this research successfully. My sincere appreciation to Kristín Björg Ólafsdóttir and Sigurbjörg Borgthórdóttir for assistance with CO_2 coulometer analysis; Dr. Thráinn Fridriksson for reviewing and giving technical advice regarding the statistical analysis of CO_2 emissions through soil; Dr. Sigurdur Reynir Gíslason for his diligent care and effort reviewing my thesis.

My gratitude to Dr. Ingvar Birgir Fridleifsson, the Director and Mr. Lúdvík S. Georgsson, deputy director of UNU-GTP for giving me the opportunity to attend the Programme and for their encouragement and guidance throughout the entire course; Ms. Thórhildur Ísberg, Ms. Dorthe H. Holm and Mr. Markús A.G. Wilde for their support and important cooperation.

I am indebted to the staff of Lageo S.A. de C.V.: Ms. María Inés Magaña for providing CO_2 flux data; Ms. Claudia Molina de Padilla for samples preparation and shipping; Ms. Elizabeth de Henríquez, Mr. Kevin Padilla, and Mr. Emilio Guerra for giving valuable technical advice and comments regarding my thesis; Mr. Wilmer Guevara and Mr. José Tenorio for chemical data of well fluids and steam vents; Mr. Aníbal Rodríguez for physical data of well fluids; Mr. Ricardo Medrano for maps and images; and Ms. Guadalupe de Perdomo and Mr. Marco Tulio Torres for ensuring technical documents are available.

ABSTRACT

Two processes of carbon dioxide removal from geothermal systems have been studied as part of the CO_2 budget in the Berlin geothermal system and their implications for the evaluation of the CO_2 emissions from a 109 MWe geothermal power plant. CO_2 flux through soil was measured as part of natural emissions at 150 sampling points within a regular grid of 4 x 2.5 km using the accumulation chamber method. Results were analyzed by a graphical statistical method. Soil CO_2 flux values over background values were not observed and characterization of the CO_2 source feeding the soil CO_2 diffuse degassing was not possible due to the amount of volcanic-hydrothermal CO_2 and biogenic fluxes that coexist and are of the same order of magnitude. The rate of CO_2 emissions through an area of 4 x 2.5 km was from 14162 to 23105 t y^{-1}. The amount of CO_2 fixed in bedrock was quantified by coulometric carbon titrations of 50 drill cutting samples from 5 high temperature geothermal wells in the southern region of Berlin. The amount of CO_2 in the drill cuttings ranged between 0.0 and 194 kg m^{-3}. For wells located in the westernmost region the CO_2 content reaches the highest values in the uppermost 1200 m but it decreases sharply below that depth and very little CO_2 is present in minerals below 1500 m. A more homogeneous CO_2 distribution has been observed in wells located in the eastern part of the area studied where CO_2 content of the order of 60 kg m^{-3} was found at 1845 m depth. The load of the bedrock was computed to be 79.5 kg m^{-2} and the total amount of CO_2 fixed in the bedrock was estimated as 795 Mt. The CO_2 fixation rate of the system was computed to be between 6100 and 79500 t y^{-1}. CO_2 emissions from the power plant amounted to 42420 t y^{-1} in the year 2008, double the natural emissions observed in the present study.

TABLE OF CONTENTS

LIST OF FIGURES

LIST OF TABLES

LIST OF SYMBOLS

A	Surface area of accumulation chamber (m^2)
a	Activity coefficient
°C	Degrees Celsius (°C)

d	Number of months operating by a turbine during one year
E_y	CO_2 emissions per year (t_{CO2}/year)
F_{CO2}	Total CO_2 output from an area surveyed (t y^{-1})
g kWh^{-1}	Grams per kilowatt-hour
Gt	Gigatones (10^9 tones)
GWh	Gigawatt-hour (GWh)
K	Equilibrium constant
Kac	Accumulation chamber factor (mol m^{-2} d^{-1} ppm^{-1} s)
Kc	Accumulation chamber calibration constant
m	Slope of the curve ($\Delta C/\Delta t$)
M	CO_2 arithmetic mean (g m^{-2} d^{-1})
Ma	Megaannum: million years ago
MN	CO_2 flux Arithmetic median (g m^{-2} d^{-1})
$M_{s,y}$	Mass of steam used for electricity generation per year (tones/year)
Mty^{-1}	Megatonnes per year (10^6 tones/year)
MWe	Megawatt electric (10^6 watts)
pCO_2	Partial pressure of CO_2
P	Barometric pressure (mbar)
ppm	parts per million
R	Gas constant 0.08314510 (bar L/mol K)
S	Surface area (m^2)
T	Air temperature in degrees K
µg	Microgram (10^{-6} grams)
µm	Micrometer (10^{-6} m)
V	Volume of the accumulation chamber (m^3)
TVD	Total Vertical Displacement (m)
%T	Transmittance percentage
w^{ave}_{CO2}	Mass fraction average in steam per month (t_{CO2}/t_{steam})

Acronyms, initialisms

BP	Before present
CEL	Comisión Ejecutiva Hidroeléctrica del Rio Lempa
GENZL	Geothermal Energy New Zealand Ltd.
GESAL	Geotérmica Salvadoreña S.A. de C.V.
GEW	Gram equivalent weight
MT	Magneto-Telluric
NDIR	Non-dispersive Infrared
PNUMA	Programa de las Naciones Unidas para el Medio Ambiente
SIGET	Superintendencia General de Electricidad y Telecomunicaciones

Greek letters

Φ_d	Steady state diffusive flux
ν	Soil porosity
D	Diffusion coefficient
Φ_a	Advective flux
k	Specific permeability
µ	Fluid viscosity
σ	Standard deviation
$\delta^{18}O$	Oxygen 18 isotope in delta notation ($\delta = [(R_{sample} - R_{standard})/R_{standard}]\times 1000$. $R = {}^{18}O/{}^{16}O$. Standard is SMOW (Standard Mean Ocean Water).
$\delta^{2}H$	Deuterium isotope in delta notation. $R = {}^{2}H/{}^{1}H$Standard is SMOW.
$\delta^{13}C$	Carbon 13 isotope in delta notation. $R = {}^{13}C/{}^{12}C$. Standard is PDB (Pee Dee Belemnite)

1. INTRODUCTION

Geothermal energy is generally accepted as being an environmentally benign energy source, (Hunt, 2000). Release of carbon dioxide gas (CO_2) to the atmosphere is commonly considered to be one of the negative environmental effects of geothermal power production, even though it has been shown to be considerably less than from fossil fuel power plants (Ármannsson et al., 2005). High temperature geothermal systems generally occur in areas of active volcanism where the heat source may be a major magma intrusion, a dyke complex, or a complex of minor intrusions (Arnórsson et al., 2007). Studies of CO_2 emissions from geothermal/volcanic systems have demonstrated that vast quantities of CO_2 are released naturally and that, in many cases, natural emissions far exceed emissions form geothermal power production (Delgado et al., 1998).

Carbon dioxide in volcanic geothermal systems has a magmatic origin as the primary source but may also be derived from other sources, such as metamorphism of carbonate rocks. Processes that remove CO_2 from geothermal systems are atmospheric emissions, calcite precipitation, and dissolution in enveloping ground waters (Mörner and Etiope, 2002; van Loon and Duffy, 2005).

Comprehension of CO_2 budget of geothermal systems has implications for the evaluation of the environmental impact of geothermal power production. It has been argued that the initial increase in CO_2 emissions from a new geothermal power plant will be counteracted by decreased natural emissions in the future. (Bertani and Thain, 2002); on the other hand, Sheppard and Mroczek (2004) based on heat-flow measurements as a proxy for gas-flow measurement, suggest that exploitation of the Wairakei geothermal system, New Zealand, has resulted in significantly increased diffuse CO_2 discharge from the field, i.e., of the same order as from the power station itself.

Several recent soil gas surveys have shown high CO_2 concentration over faults and fractures in different geological settings (Mörner and Etiope, 2002). Significant amounts of CO_2 are released to the atmosphere by both direct volcanic emanations and soil diffuse degassing from volcanic geothermal systems.

Measurements of CO_2 efflux are also applicable in some tectonic areas because they are useful in the identification of active faults and crevasses for the location and evolution of hydrothermal fluids. At some locations, dissolved CO_2 in groundwater can be a significant component of the total volcanic efflux (Sorey et al., 1998). Faults may act as conduits for gas and water flow from depth.

Several studies have been performed in Iceland in order to estimate the total CO_2 emissions from Icelandic geothermal systems, the computed values ranged between 1 to 2 Mt/year (Arnórsson and Gíslason, 1994; Ármannsson et al., 2005). In the Reykjanes geothermal area Fridriksson et al. (2006) measured the natural CO_2 emissions concluding that more than 97% are released through soil environment as diffuse degassing and that the vent emissions are only a small fraction of the total emissions.

Ármannsson et al. (2007) have studied the CO_2 fixation by calcite in high-temperature geothermal fields in the Krafla geothermal field and Wiese et al. (2008) at Reykjanes, Hellisheidi and Krafla geothermal fields, Iceland, respectively. The amount of CO_2 fixed in bedrock was quantified in order to determine the importance of CO_2 fixation in rock to the CO_2 budget of geothermal systems.

Additionally, emissions from Icelandic power plants amounted to 0.16 Mt/year in 2004 (Ármannsson et al., 2005) which are considered significant compared to the total estimated emissions. This argument is of great importance in countries like in El Salvador where the geothermal contribution to the electricity budget is presently 25%.

Quantification of the relative magnitudes of the fixation of CO_2 in calcite and groundwaters, on the one hand, and natural atmospheric emissions on the other, can be considered as a natural experiment to determine the capacity of bedrock to capture CO_2. The present study focuses on the estimation of the capacity of bedrock in the Berlin geothermal field to capture CO_2 and involves two steps:

a) Quantification of CO_2 fixation in calcite by total carbon measurements in drill cuttings from high temperature geothermal wells.
b) The study of CO_2 degassing through soil flux measurements in order to determine its contribution to the natural CO_2 budget of the atmosphere.

2. GEOTHERMAL DEVELOPMENT

Exploration for geothermal resources in El Salvador began in the mid-60´s with the aid of the United Nations. Campos (1981) stated that 18 geothermal areas have been identified in the country and these were classified as low and high enthalpy areas. Technical studies in El Salvador have been focused on power generation. The main characteristics of high temperature geothermal systems of El Salvador are listed in Table 1.

Geothermal energy production in El Salvador dates back to 1975, with the first 30 MWe unit in Ahuachapán. Today there are two geothermal fields in operation: Ahuachapán and Berlín with an installed capacity of 95 MWe and 109 MWe, respectively. Geothermal power production has increased from 400 GWh in 1995 to 1293 GWh in 2007. The geothermal resources provide 25% of the electricity market of the country (SIGET, 2008).

The Berlín Geothermal Field is one of the major geothermal fields in the country, located approximately 110 km ESE of the city of San Salvador, with an area of 12 km x 16 km at a mean elevation of 800 metres above sea level (m a.s.l.), and is a water-dominated system with temperature close to 300°C in the production zone.

TABLE 1: High temperature geothermal systems in El Salvador, mean reservoir temperature in °C and reservoir volume in km^3 (modified from Campos, 1981)

Name of area	Field	Mean reservoir temperature (°C)	Mean reservoir volume (km^3)
Ahuachapán	Ahuachapán San Lorenzo Chipilapa	233 ± 6 216 ± 22 231 ± 4	10 ± 2 2 ± 1 10 ± 2
Usulután	Berlin	316 ± 6	10 ± 4
San Vicente	San Vicente	228 ± 10	14 ± 6
San Miguel	Chinameca Chambala	210 ± 8 233 ± 10	10 ± 3 3 ± 1
Santa Ana	Coatepeque	216 ± 5	9 ± 3
Sonsonate	Caluco	207 ± 25	2 ± 1
La Unión	Conchagua	180 ± 12	2 ± 1

The stepwise development of Berlin started when the first exploration well (TR-1) was drilled in 1968, production from the system started in 1992 with two 5 MWe backpressure units. In 1999, 18 additional wells were drilled and two 28 MWe condensing units went on line. On December 2005, a third condensation unit, 44 MWe, went on line and 9 new wells were drilled in the south region of the geothermal field within the frame of a new exploration project, which has the aim to investigate the boundary of the field.

To date 39 wells have been drilled in the Berlin field, of which 14 are production wells with an average steam fraction of 22% and an average measured enthalpy of 1240 kJ/kg with the exception of well TR-18 A which is 100% steam with an enthalpy of 2,800 kJ/kg. The number of drilled wells is completed by 19 injection and 6 abandoned wells (Rodríguez and Monterrosa, 2007). A binary unit went on line in 2008, and that will increase the power generation capacity by 9.2 MWe with the conversion of thermal energy of low pressure geothermal brine into electrical energy.

The current installed capacity is 109 MWe; the gross production capacity is 104 MWe with a fluid mass extraction of 780 kg s^{-1} (205 kg s^{-1} steam and 575 kg s^{-1} liquid). The total brine is injected at an average temperature of 143°C in the northern part of the field.

Figure 1 depicts the location of the Berlin geothermal field as well as its main geological structures and geothermal wells.

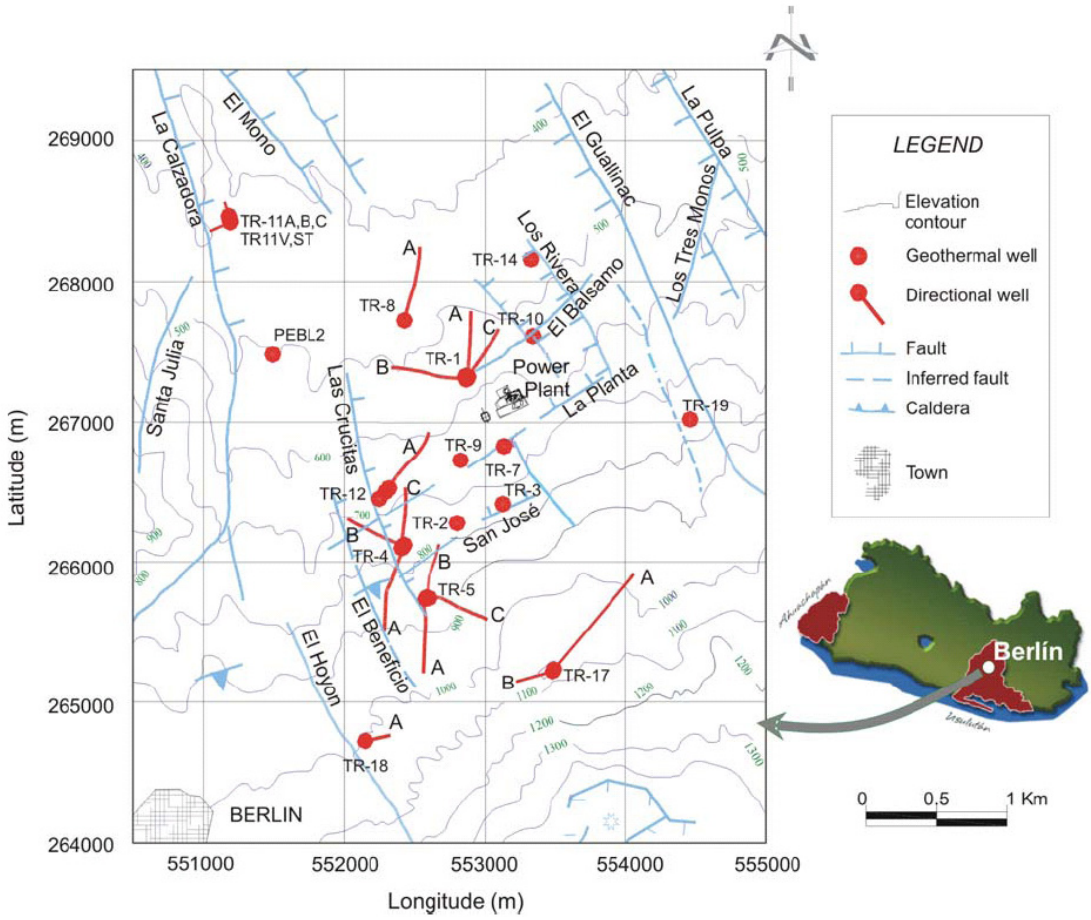

FIGURE 1: Main structures and well location for the Berlin geothermal field

3. GENERAL FEATURES OF THE AREA STUDIED

3.1 Geological features

The region shows a compressive stress due to the oblique subduction of the Cocos plate under the Caribbean plate defined by the Middle American Trench (Molnar and Sykes, 1969) where the volcanic chain runs WNW-ESE, parallel to the coast as depicted in Figure 2. The active volcanic chain in El Salvador is aligned with the southern margin of the Median Trough, which is a normal graben formed during the Plio-Pleistocene. This graben crosses El Salvador and continues parallel to the Middle American Trench. Different hydrothermal manifestations occur along the volcanic chain.

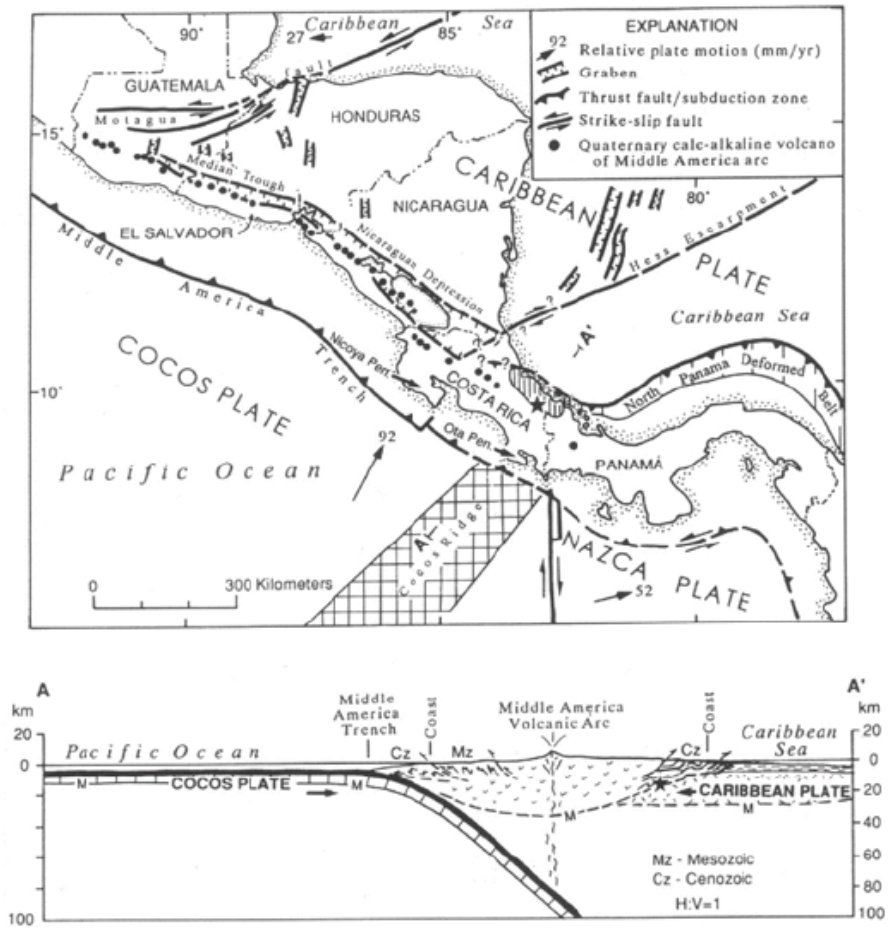

FIGURE 2: Geodynamic sketch of Central America. Cross section trends SW (A) to NE (A´) (modified from Lageo, 2004)

Four fault systems have been recognized in Berlin (CEL, 1996). The WNW-ESE system is associated with the formation of the Central Graben. The NW-SE and NNW-SSE systems are considered the most recent and active, allowing for the ascent of geothermal fluids from depth to the surface, and most hydrothermal manifestations occur along the structure of the NNW-SSE graben.

3.2 Volcanology

Two stages of activity are characteristic of Central-American volcanism, both of them separated by a long lull. The former dates back to > 3 Ma, and led to the formation of the so-called basement (Balsamo formation). The latter developed about 1 Ma ago and is still active.

The existence of two calderas has been suggested for this system. The Berlín volcano was formed 1.4 million years ago (CEL, 1996) followed by the formation of the Berlín Caldera 0.1 million years ago which collapsed with the formation of a NW-SE graben. The formation of a second caldera after a Plinian eruption has been suggested (caldera Blanca Rosa) 75,000 years ago. The more recent volcanic products belong to the Tecapa Quaternary volcanic complex, with the most recent eruption only 700 BP. This recent phreatomagmatic activity vented from the El Hoyón crater SW of the study area (CEL, 1996).

There is an alternation of basaltic to andesitic lava flows and scoria, and andesitic to dacitic ignimbrites, which were produced during major eruptions (GESAL, 2001). The basaltic rocks date as 1.4 Ma old, whereas the andesitic-dacitic ignimbrites date from 0.1 to 0.075 Ma ago.

Since the present lavas in the Berlin volcanic system have an andesitic-basaltic composition, and due to the fact that atmospheric CO_2 fixation rates are strong functions of the Si:O ratio of the rock (see Wolff-Boenisch et al., 2004 and 2006), the relative long-term CO_2 consumption capacity of the Berlín rocks could be two orders of magnitude higher than those of rhyolite composition, playing an important role in long-term atmospheric CO_2 evolution.

The Berlín geothermal field is related to the Berlín-Tecapa volcanic complex and the Berlín caldera which are of Holocene age. The magma chamber of this volcanic complex is considered to be the source of heat for the geothermal systems.

3.3 Hydrothermal alteration

Four mineral alteration zones have been distinguished on the basis of the abundance and appearance of characteristic hydrothermal minerals. The shallowest alteration zone is characterized by the presence of relatively low temperature minerals, such as saponite, montmorillonite, heulandites, etc. At greater depth, hydrothermal phases, such as epidote, wairakite, prehnite and hydro-garnets typical of higher temperature conditions occur. Quartz, calcite and chlorite are widespread in most of these zones (Ruggieri et al., 2006).

Tables 2 and 3 show mineralogical facies in wells TR- 17 and TR-18 drilled in the Berlin geothermal field between July 2003 and February 2005. Thin layer and petrographical analysis of drill cutting and cores has been used for the identification of lithological units of the Berlin bedrock. Besides correlation of mineralogical temperatures defined by fluid inclusions as well as by measured temperatures is also shown.

TABLE 2: Mineralogical facies in wells TR-17 Berlin geothermal field (modified from Lageo, 2008a)

Facies	Indicator Mineral	TR-17	TR-17A	TR-17B	Temp (°C)
Argillitic	Smectite, oxides, < Ca, Si, << Quartz, < Corrensite < Heulandite, Clinoptilolite, Epistilbite	0-370 m	0-350 m	0 – 380 m	50 - 120
Argillitic-Phyllic	Smectite, oxides, Corrensite, Calcite, <Chlorite, <Quartz	370-690 m	350–710 m	380-700 m	120-180
Phyllic	Calcite, Chlorite, <Pennine, Quartz <Epidote, Prehnite, Anhydrite < Wairakite	690–1040 m	710-1150 m	700-1150 m	180-220
Phyllic-prophylithic	Calcite, Chlorite, Pennine, Quartz, Wairakite Epidote, Prehnite, Illite,	1040-1320 m	1150-1550 m	1150-1260 m	220-260
Prophylithic	Chlorite, Pennine, < Calcite, Wairakite, >>Epidote	1320-2422 m	1550-2690 m		>260

3.4 Petrography

The stratigraphic succession for the Berlin area includes 4 units starting from the surface down.

i) Unit I. Andesitic lava and argillaceous pyroclastic rocks

TABLE 3: Mineralogical facies in wells TR-18 Berlin geothermal field (modified from Lageo, 2008a)

Facies	Indicator Mineral	TR-18	TR-18A	Temp (°C)
Argillitic	Smectite, oxides, < Ca, Si, << Quartz, < Corrensite <Heulandite, Clinoptilolite, Epistilbite	0-240 m	0-200 m	50 – 120
Argillitic-Phyllic	Smectite, oxides, Corrensite, Calcite, Chlorite, Quartz	240-600 m	200-620 m	120-180
Phyllic	Calcite, Chlorite, < Pennine, Quartz < Epidote, Prehnite, Anhydrite < Wairakite	600 – 1300 m	620-1138.5 m	180-220
Phyllic-prophylithic	Calcite, Chlorite, Pennine, Quartz, Wairakite Epidote, Prehnite, Illite,	1300 - ?m		220-260
Prophylithic	Chlorite, Pennine, < Calcite, Wairakite, >>Epidote	?m – 2600 m		>260

ii) Unit II. Pyroclastic rocks of different types. They contain quartz and calcite growing structures associated with haematite. Mineralisation makes up 10-30% of the rock. Andesitic lava with Carlsbad twinned plagioclase (33-50%) has mineralized with calcite in both the matrix and the veins.

iii) Unit III. Pyroclastic rocks with Epidote (5-20%) in veins and fractures and with calcite + quartz in fractures. Altered andesitic-basaltic lava.

iv) Unit IV. Andesitic lava with Epidote + chlorite (>20%) in veins fractures.

The succession of alteration facies is generally not in agreement with the stratigraphic grouping into geological units since it depends on the fluid circulation and temperature experienced by the rock and not just on its lithology (Arias et al., 2003).

3.5 Geophysics

A shallow horizontal conductor with a resistivity of a few ohm-m and a thickness of some thousand meters can be identified. This conductor appears everywhere above the elevations where productive zones have been found; it looks narrower and arched upwards in the areas of current geothermal production (see Figure 3, MT profile).

At a fixed elevation, the geothermal environment is characterized by resistivity values higher than those for the surrounding environment. The resistivity of the production area increases with depth and reaches values between 30 and 100 ohm-m at the main productive horizon of -1100 m a.s.l. At greater depths, resistivity generally increases, although a vertical low resistivity zone (15-20 ohm-m) is visible on the west side. The deep vertical conductor could be associated with an interesting zone characterized by a greater contribution of high temperature saline fluids.

It has been suggested (Arias et al., 2003) that the passage to medium-resistive areas (between 30 and 100 ohm-m) below the shallow horizontal conductor can instead mark both the beginning of the prophylithic alteration facies and the transition to areas where andesitic lava becomes prevalent.

Gravimetric surveys show that the Berlín geothermal field belongs to the regional “high gravity” associated with the volcanic belt and is found in its NW portion (Arias et al., 2003). The first order residual Bouguer anomaly confirms the correspondence between the local gravimetric high and the geothermal reservoir. Outside this gravimetric high, the reservoir probably gets deeper and the wells are prevalently unproductive.

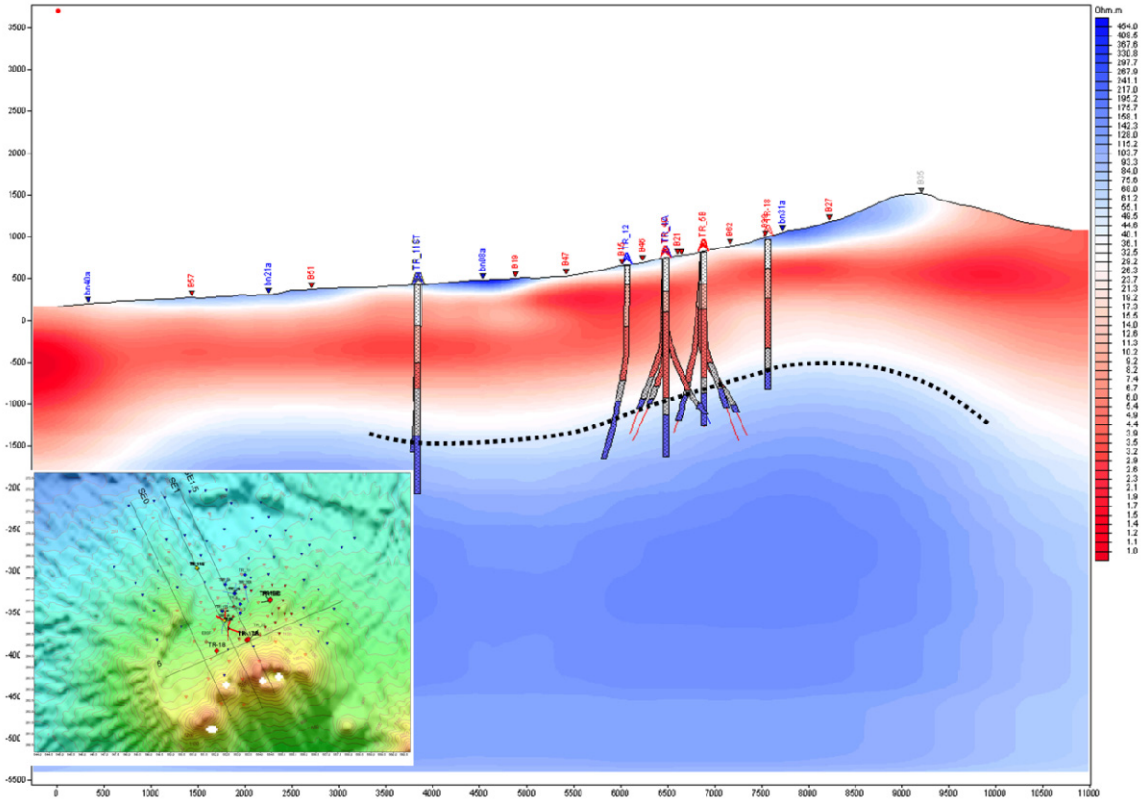

FIGURE 3: MT profile for the Berlin geothermal field
NW-SE cross section (modified from Arias 2003

3.6 Petrophysics

The available data comprise laboratory measurements of core samples collected during drilling of deep wells and have been arranged by each lithostratigraphic Unit described in section 3.4 for the Berlín geothermal field (CEL, 1987). Measured values show a trend of increase in matrix density values going from shallower to deeper Units and less markedly, in bulk density values as well. At higher depths the pattern is different; the matrix density tends to decrease slightly from 2.66 to 2.58 g/cm^3, while the bulk density continues to increase slightly from 2.34 to 2.37 g/cm^3. On the other hand porosity is characterized by mean values ranging from 10 to 13% for the first three units while those for Unit IV (i.e. the reservoir) exhibit a lower porosity, 9-10%.

3.7 Geochemistry

The reservoir fluids are NaCl waters with about 5000-11000 mg/kg of total dissolved solids, 3000 to 6000 mg/kg of chloride, and 600 to 900 mg/kg of silica. The concentration of non-condensable gases in the steam is in the 0.25-0.50% range by weight, with CO_2 constituting 80 to 90% of the total gas. CO_2 concentrations in the reservoir fluids are usually between about 200 and 1900 mg/kg with partial pressures (P_{CO2}) of 0.49-4.60 bar (D´Amore and Mejia, 1998). The low CO_2 content cannot be explained by a boiling process only (Arias et al., 2003) but it seems to be related to a poor gas flow from depth or the absence of complete equilibrium due to different permeability boundaries. Several fluid circulation patterns, providing different levels of water-rock interaction should be considered as another possibility.

Temperature values for geothermal wells at initial conditions have been estimated by D´Amore and Mejia (1998); the average equilibrium temperature ranged from 305°C at well TR-5 to 241°C at well TR-10. Computed gas geothermometer results reflect temperatures ranging from 240°C in well TR-1 to 305°C in well TR-9. Saturation indices at initial conditions in the Berlín geothermal system are very close to showing calcite saturation (D´Amore and Mejia, 1998).

The salinity and enthalpy differences between the reservoir fluids from individual wells have been explained in terms of fluid mixing, boiling and conductive cooling (D'Amore and Mejia, 1998). Fluid enthalpy varies between 1200 and 1400 kJ/kg, measured temperatures in the production zones are in the range 254-300°C, while lower values, around 245-250°C, were observed in the northern part of the field where the wells are utilized for reinjection purposes.

The N_2/Ar molar ratio in well gas (15-22) is very close to that of ground water equilibrated with air at 25°C. The isotope composition (δ^2H and $\delta^{18}O$) of the geothermal fluids confirms their meteoric origin. The same liquid phase feeds the fumaroles and wells located at Berlin. Fumarolic gas concentration depends on the percentage of steam condensation as they rise to the surface; in general, the farther the manifestations are from the main up flow, the highest the gas content.

3.8 Conceptual model

The heat source feeding the geothermal system is related to the residual heat of the magmatic chamber which originates in the Berlin caldera and more likely to the more recent post-calderic magmatic chamber (Figure 4). The heat source is located under the Berlin-Tecapa volcanic complex; the recharge of the system is meteoric in origin and this has been corroborated by isotope analysis and is due to the highly fractured structures and the annular faults which played the role of hydrological barriers to secure the recharge of meteoric water inside de caldera. The up flow comes from the south inside the caldera and the hot fluid moves towards to the north along the graben structures.

Three types of aquifer have been identified based on chemical data: a low salinity aquifer of 1600 ppm at a depth between 200 and 300 m a.s.l.; (2) an intermediate-salinity aquifer with a salinity of 6600 ppm at sea level; (3) a deeper saline aquifer with a salinity between 8000 and 12000 ppm at a depth of -800 to -1200 m a.s.l. (Electroconsult Spa, 1994). The geothermal reservoir is located within a layer of andesitic to andesitic basaltic lavas and tuffs belonging to the Tertiary basement.

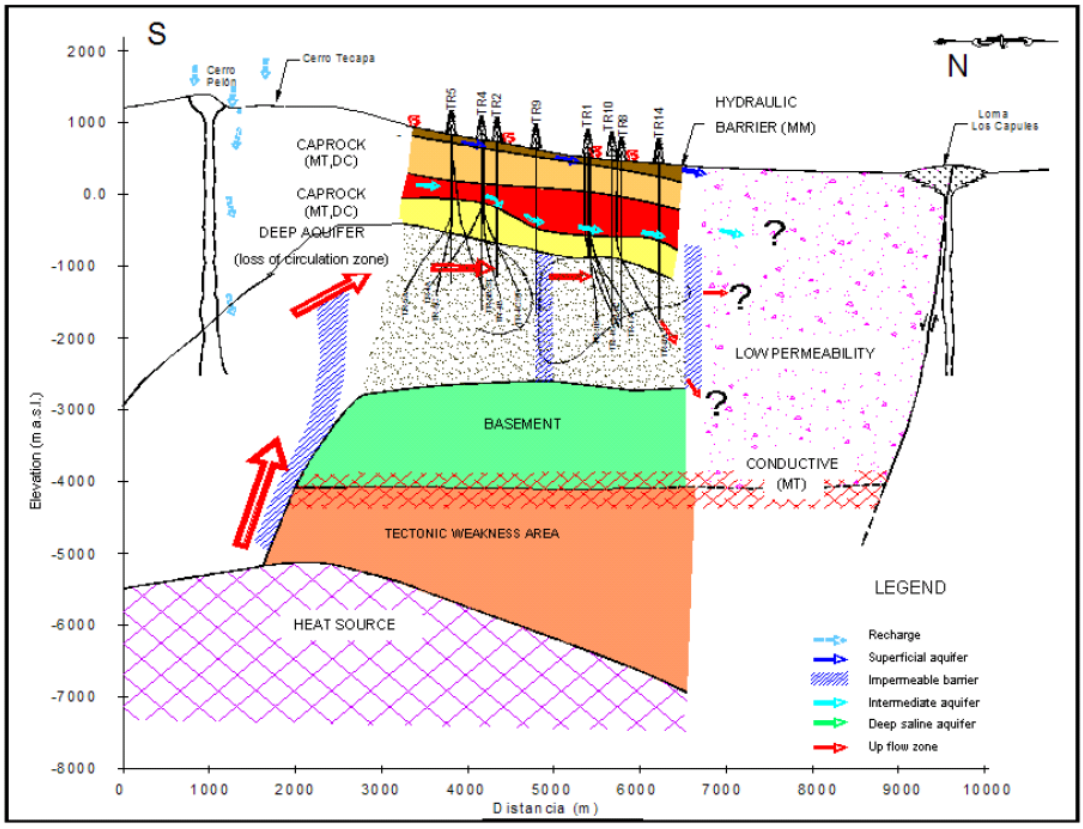

FIGURE 4: Schematic description of the Berlin conceptual model.
N-S cross section (Monterrosa, 2002)

4. SAMPLING AND ANALYSIS OF GEOTHERMAL FLUIDS

4.1 Sample collection

Carbon dioxide concentration was measured in water and steam phases from selected geothermal wells, as well as in the steam phase from a humidity separator (demister).

For geothermal wells, steam and water samples were collected at the same pressure using either a Webre separator or sampling ports installed at the cyclonic separator. In the cases of wells TR-17, 17A and 17B, sampling points are located on the two-phase pipeline approximately 20 m ahead of the wellhead (Lovelock and Stowell, 2000; Lovelock, 2001). For samples collected from well TR-17 in September 2008 and January 2009 the selected sampling point was at the wellhead. For wells TR-18 and TR-18A, samples were collected from the cyclonic separator as each well is connected to its own separator.

In the case of steam samples collected at the demister a stainless steel condenser which has previously been connected to the sampling port located in the steam pipeline at the entrance of the turbine was used. It was assumed that the amount of gas present at this point is representative of the CO_2 emissions from the power plant.

Steam samples were collected in duplicate into evacuated gas sampling bulbs containing 50 ml of a 4N NaOH solution.

Water samples from geothermal wells were collected at the same pressure as steam samples and filtered through 0.2 μm cellulose acetate membrane filters into high density polyethylene bottles using a filter holder of the same material. The sample is split into two portions, 500 ml each; one of them is preserved adding 2.5 ml of suprapure concentrated HNO_3 for the analysis for major cations (Na, K, Ca, Mg), boron and silica; the second portion is used for pH, chloride, and total carbon dioxide and sulphate analysis.

4.2 Analysis of water and steam samples

The concentration of NaOH soluble CO_2 was determined by titration with 0.1M HCl standard solution (Giggenbach and Goguel, 1989; Nicholson, 1993).

In water samples, total carbon dioxide and pH were determined in the laboratory after sampling by titration with 0.1M HCl. Interference from other bases was corrected for by back titration with 0.1M NaOH following the bubbling of N_2 through the solution to remove dissolved gases from the sample (Pang and Ármannsson, 2006). Potentiometric titration with 0.01N $AgNO_3$ was used for chloride analyses. Ion chromatography was used to determine sulphate. The major aqueous cations plus silica and boron were analyzed for on a VARIAN AAS.

5. FLUID COMPOSITION

5.1 Theoretical estimation of the representative CO_2 concentration in steam

The carbon dioxide in the geothermal fluid is mostly of magmatic origin. On the basis of $\delta^{13}C_{(CO2)}$ and $\delta^{13}C_{(CH4)}$ values for the Berlin fluids at initial producing conditions, D´Amore and Tenorio (1999) suggest that evidence for a component of andesitic magma is present.

Some of the CO_2 may be derived from the carbon in the rock undergoing alteration at depth. During the lifetime of geothermal systems, a fraction of the carbon at deep levels may accumulate in the hydrothermally altered rock in the upper part of the geothermal system as carbonate minerals.

The chemical equilibria and physical characteristics of the fluid in the reservoir seem to be responsible for the observed concentrations of the main reactive gas species found in the fluid from high-temperature geothermal systems (D´Amore and Truesdell,1985; Arnórsson and Gunnlaugsson, 1985). This indicates that the activity of dissolved gases such as CO_2 is controlled by a close approach to equilibrium with specific mineral buffers, at least prior to utilization. At temperatures above 230°C epidote + prehnite + calcite + quartz are considered to buffer CO_2. The equilibrium reaction is:

$$2Ca_2Al_3Si_3O_{12}(OH) + 2\,CaCO_3 + 3SiO_2 + 2\,H_2O \leftrightarrow 3\,Ca_2Al_2Si_3O_{10}(OH)_2 + 2CO_{2,\,aq} \qquad (1)$$

Assuming that the activity of calcite, quartz, and water is equal to unity, the logarithm of the activity of dissolved CO_2, $a_{CO2,aq}$, can be expressed as:

$$\log a_{CO2,aq} = 1/2 \log K + \log a_{czo} - 3/2 \log a_{pre} \qquad (2)$$

Upon utilisation, the CO_2 concentration in the aquifer fluid may change affecting the fluid discharged from the wells. Several causes have been identified regarding the previously mentioned changes. In the case of the Berlin system, mixing processes in up flow zones, different permeability boundaries and fluid circulation patterns have been considered.

5.2 Calculation of aquifer composition

Table 1 in Appendix 1 shows the water and gas compositions used as input for the WATCH chemical speciation program (Arnórsson et al. 1982; Bjarnason, 1994), version 2.1. The deep fluid composition was calculated using the quartz temperature as reference temperature and was based on two assumptions: firstly that phase equilibrium exists between the steam and water phases in the reservoir; secondly, samples at the wellhead are mostly fluids derived from the vaporization of the liquid phase existing in the reservoir (Arnórsson et al., 2000; Arnórsson et al., 2007). The reservoir temperatures computed for each sample, were consistent with measured temperatures in the wells (Lageo, 2009). Table 4 shows CO_2 concentration in the total discharge at sampling pressure as well as the CO_2 concentration in the vapour phase and steam fraction produced by adiabatic boiling from the reference temperature to 100°C. The average concentration of dissolved CO_2 in the deep fluid ranges from 226.4 for well TR-17A to 585.3 for well TR-18. The steam fraction produced by adiabatic

TABLE 4: Calculated CO_2 concentration in the aquifer at total discharge and after adiabatic boiling in one step to 1 bar

WELL	DATE	CO_2 (mg/kg) Liquid [1]	CO_2 (mg/kg) steam[2]	Steam Fraction[2]
TR-17	16/11/06	432.6	1293.73	0.3341
	21/05/07	490.73	1327.21	0.3696
	23/01/08	463.86	1270.63	0.3648
	13/01/09	474.9	1291.87	0.3674
TR-17A	28/08/07	259.09	822.16	0.3148
	27/09/07	202.09	731.52	0.2758
	23/01/08	217.04	765.56	0.2831
	31/03/08	227.24	786.4	0.2885
TR-17 B	08/12/06	429.86	1340.28	0.3204
	24/01/07	431.09	1350.13	0.3188
	18/02/08	458.34	1455.3	0.3145
	13/01/09	448.57	1387.23	0.3231
TR-18	17/09/07	540.38	1771.34	0.304
	31/03/08	630.52	1991.15	0.3156
	27/05/08	578.42	1911.74	0.3017
	12/08/08	592.06	1943.47	0.3034

[1] CO_2 concentration in the aquifer fluid at total discharge
[2] CO_2 concentration and stem fraction in the aquifer assuming adiabatic boiling in one step to 1 bar (100°C)

boiling from reference temperature to 100°C is on average 0.319 with 0.290 as minimum in well TR-17A and 0.359 the maximum in well TR-17. These values were computed assuming a degassing coefficient of 1.The CO_2 concentration in the steam phase will be on average 1340 mg/kg.

5.3 Calcite saturation index

The computer code WATCH gives the saturation index (SI) for selected hydrothermal minerals at selected temperatures. Appendix 2 shows the saturation indices for calcite vs. temperature for the production wells TR-17, TR-17A, TR-17B and TR-18.

Wells TR-17A and TR-18 have experienced a calcite SI increase since they started producing in May 2007 and January of 2007 respectively. The rest of the wells reveal undersaturation conditions up to today.

Well TR-17A shows a calcite SI increasing tendency during the first six months of production without reaching supersaturation. During the year 2008, SI reaches values as high as 0.5-0.6. On the other hand, well TR-18 an increase tendency in SI is observed since the beginning of production. Calcite SI values ranged between 0.33-0.42 which are representative of supersaturation conditions in this well.

6. CO_2 EMISSIONS FROM THE BERLIN GEOTHERMAL POWER PLANT

Since the commissioning of Unit III (44 MWe) at the Berlin geothermal field in January 2007, a monitoring program of gas emissions has been carried out. This involves collecting samples periodically, at least four times per year. The gas emission monitoring program includes steam flow rate measurements and chemical gas content. The amount of steam discharged from the geothermal wells, in kg/s units, is measured through two annubar flow meters, which are basically a Pitot tube with an electronic pressure transmitter installed in the steam pipeline after being separated from water. They are located at both platforms of the wells studied. Daily values are reported and monthly values are computed in tonnes of steam. CO_2 content in steam is computed as previously described in Section 4.2.

Carbon dioxide emissions from each of the Units at the Berlin geothermal field were computed according to the following equation:

$$Ey\ (t_{CO2}) = w^{ave}_{CO2} * M_{s,\,m} * d \qquad (3)$$

where Ey = CO_2 emissions per year (t_{CO2}/year)
w^{ave}_{CO2} = CO_2 mass fraction average in the produced steam per month (t_{CO2}/t_{steam})
$M_{s,\,m}$ = Amount of steam used for electricity production per month (t/month)
d = Number of operation months during one year

Figure 5 shows mass of steam per month used in electricity production at the Berlin power plant during the period 2007-2008. Values are specific for each Unit and the total mass is plotted in orange. Low values correspond to a maintenance program carried out for each unit. Unit I went offline for 22 days during September/08, Unit II for 35 days between April and May/07, and Unit III for 45 days between October and November/08. (Lageo 2007, Lageo 2008b). Tables 1a and 1b in the Appendix 3 show operational characteristics in the Berlin power plant.

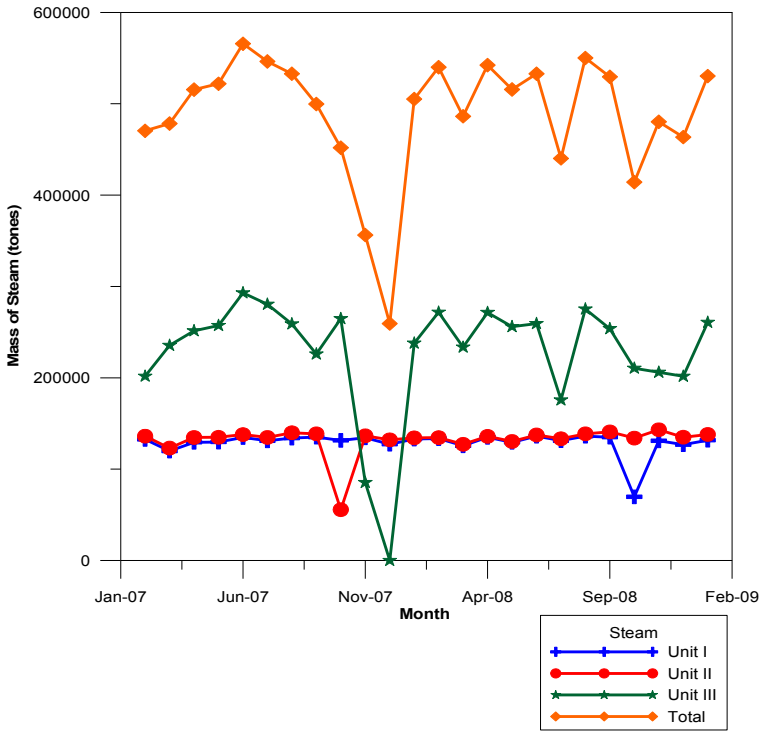

FIGURE 5: Mass of steam per month for each Unit and total steam mass in the Berlin power plant for the Period 2007-2008

Figure 6 shows both CO_2 concentration and mass fraction in steam for the three units in operation at the Berlin power plant. Gas concentration for Units I and II depicts relatively similar values which are lower than for the steam going to Unit III. The main difference is that the steam fraction of well TR-18A is 1 and its contribution to the total amount of gas is significantly higher than that of the rest of the production wells drilled in the geothermal field.

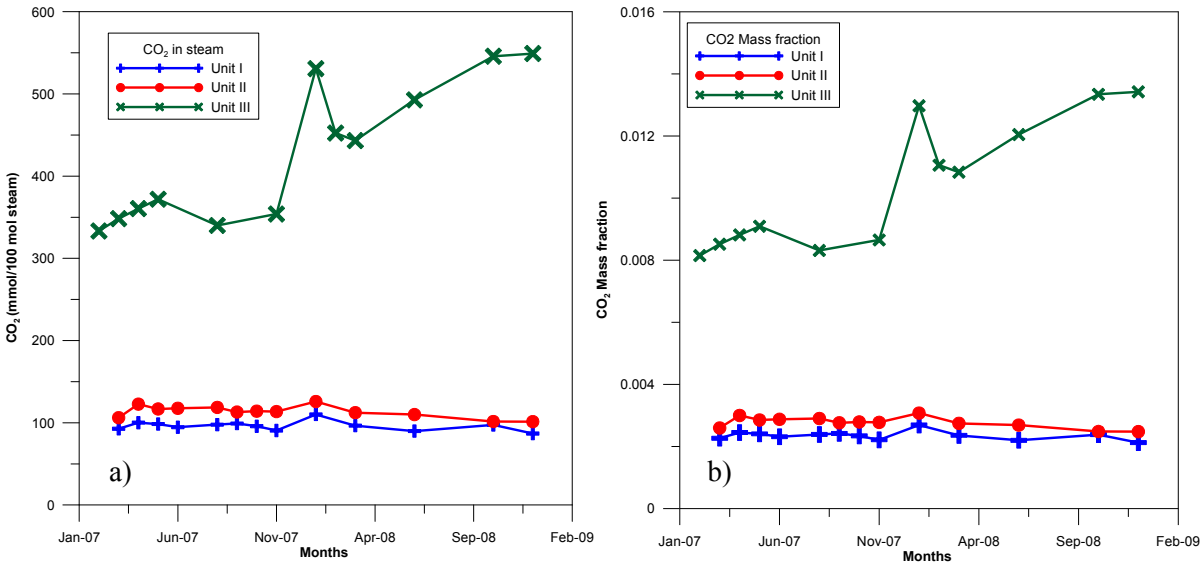

FIGURE 6: a) CO_2 analytical results in mmol/100 mol and b) CO_2 mass fraction for each Unit in the Berlin power plant for the period 2007-2008

Tables 5, 6, and 7 show selected monitoring data during the period studied. For the purpose of this study CH_4 contributions are not considered so the emissions include only a CO_2 contribution. The average value for each year, i.e. w^{ave}_{CO2} and $M_{s,m}$, where computed and then used to estimate the CO_2 emissions per year from the above mentioned Unit. Concentrations of CO_2 in steam for Units I and II have also been monitored and the results reported.

Figure 6 shows an increasing tendency in CO_2 emissions for Unit III. This is due to greater fluid extraction from well TR-18 which has been drilled in the steam zone of the geothermal field. The higher the steam extraction from this well the higher the CO_2 mass fraction in the power plant emissions.

TABLE 5: Measured values for the estimation of CO_2 emissions from Unit I in the Berlin geothermal power plant

Date	CO_2 (mmol/100 mol steam)	w^{ave}_{CO2} (t CO2/ t steam)	Ms (t steam/month)
2007			
February	92.7	0.0023	119856
April	98.43	0.0024	129727
July	97.66	0.0024	134079
October	90.6	0.0022	134441
December	110.1	0.0027	133013
Average	**97.90**	**0.0024**	**130223**
2008			
February	96.49	0.0024	125566
May	89.95	0.0022	136125
September	97.45	0.0024	69689
November	86.92	0.0021	126781
Average	**92.70**	**0.0023**	**114540**

TABLE 6: Measured values for the estimation of CO_2 emissions from Unit II in the Berlin geothermal power plant

Date	CO_2 (mmol/100 mol steam)	w^{ave}_{CO2} (t CO2/ t steam)	Ms (t steam/month)
2007			
February	106.14	0.0026	123030
April	116.72	0.0029	134875
July	118.68	0.0029	139848
October	113.57	0.0028	136498
December	125.82	0.0031	134221
Average	**116.19**	**0.0028**	**133694**
2008			
February	112.3	0.0027	127193
May	109.96	0.0027	137420
September	101.55	0.0025	133990
November	101.34	0.0025	134988
Average	**106.29**	**0.0026**	**133398**

6.1 Results

For the year 2007 the computed amount of CO_2 emissions for a gross power generation of 720.176 GWh was 30463 tons CO_2 y^{-1}. One year later annual emissions of CO_2 were estimated as 42420 tons CO_2 y^{-1}. From Figure 6, the mass fraction of CO_2 for Unit III depicts a tendency for increase since the beginning of production. In addition, Table 2 in Appendix 1 shows that the amount of steam extracted per year, increased from 5.70 to 6.03 Mt and power generation amounted to 785.167 GWh.

In order to compare the values obtained, total CO_2 emissions from the Berlin power plant have been expressed as CO_2 per kWh of net electricity generation (see Table 8).

In a study of the full-energy-chain emissions from geothermal power generation conducted in 1989 emissions equivalent to 57 g kWh^{-1} of net electricity were estimated while in two 1992 studies 40 and 42 g kWh^{-1} were estimated Hunt (2000). This is evidence that the results obtained are of the same order as data from worldwide geothermal power stations.

TABLE 7: Measured values for the estimation of CO_2 emissions from Unit III in the Berlin geothermal power plant

Date	CO_2 (mmol/100 mol steam)	w^{ave}_{CO2} (t CO2/ t steam)	Ms (t steam/month)
2007			
February	348.28	0.00851	235513
April	371.94	0.0091	257271
July	340.03	0.0083	259007
October	353.2	0.0086	264763
December	530.7	0.01297	237864
Average	**388.83**	**0.0086**	**250884**
2008			
January	462.31	0.0113	271847
March	448.49	0.0110	271503
May	473.17	0.0116	259330
September	545.84	0.0133	210546
November	549.1	0.0134	201690
Average	**495.78**	**0.0121**	**242983**

TABLE 8: CO_2 emissions per kWh from Berlin in year 2008 and major geothermal power plants in Iceland in year 2000. Icelandic data from Ármannsson (2003)

Plant	From electricity generation only	From electricity and heat production
	CO_2 (g kWh^{-1})	CO_2 (g kWh^{-1})
Berlin	57 (2008)	57
Krafla	152 (2000)	152
Svartsengi	181 (2000)	74
Nesjavellir	26 (2000)	10

6.2 The cascaded use of geothermal fluids

Icelandic emissions reported by Ármannsson (2003) have demonstrated that the CO_2 emissions per kWh are considerably reduced when thermal energy used in direct applications is counted together with electric energy illustrating that cascading use of geothermal fluids has a mitigating effect on the environment.

The Berlin geothermal field is an example of a stepwise development strategy characterized by the sustainable use of geothermal resources available in the area. In 2007 a fourth 9.2 MWe bottoming Unit was commissioned using the separated brine from Units I and II to increase the power capacity of the plant. Total CO_2 emissions from Unit IV are negligible due to the technology used in which the temperature of the brine is high enough to be used in a heat exchanger where a binary fluid with a low boiling point is vaporized and then directed through a turbine. The vapour exiting the turbine is then condensed by cold water and cycled back through the heat exchanger. The residual brine is then injected into the reservoir.

The increase in power production from Unit IV is then favourable in reducing the CO_2 emissions. Computed values including power generation from Unit IV (4.265 GWh in 2007 and 16.195 GWh in 2008) are 42.05 and 52.93 g CO_2 kWh^{-1}.

7. CARBON DIOXIDE FLUXES

7.1 Theoretical aspects of carbon dioxide fluxes

The release and movement of volcanic gases from the magmatic chamber to the earth´s surface takes place in two ways: through the main volcanic conduit if the volcano is actively degassing with a gas plume, or transferred from the magmatic system through the surrounding hydrothermal environment. The fraction of gas that has not reacted with the aqueous solution and rocks along the path is finally released at the soil-air interface. If no interaction of gas with solid surfaces is assumed and the interfering phenomena are neglected, gases can be transported throughout the rocks and soils by two main mechanisms: (1) diffusion, due to a gradient in concentration, and (2) advection (and dispersion) where the gas is transported by a moving phase (Chiodini et al, 1998). However, the volcanic soil degassing is the combination of diffusive and advective gas transfer throughout the volcanic edifice (excluding the volcanic pipe). (López et al., 2004a).

The steady state diffusive flux Φ_d is proportional to the concentration gradient, $dC/d\lambda$, as expressed by the Fick´s first law:

$$\Phi_d = - \nu D \, (dC/d\lambda) \qquad (4)$$

where ν and D represent soil porosity and diffusion coefficient respectively, and the minus sign indicates that gas molecules move from points of high concentration towards points of low concentration (or partial pressure).

On the other hand, advection involves the movement of matter due to the action of a force, i.e. a pressure gradient $dP/d\lambda$ and is described by Darcy´s law:

$$\Phi_a = (k/\mu)(dP/d\lambda) \qquad (5)$$

where k is the specific permeability and μ is the viscosity of the fluid. Although Equation 5 was experimentally derived for the steady flow of liquids in porous media, it has been extensively used also to describe the advective flow of compressible fluids in porous media. Because of mathematical complexities, steady flow of gases has been studied assuming that they are incompressible. Although this assumption might seem unreasonable, it is justified when the pressure gradient is comparatively small.

A direct method has been used for measuring the soil CO_2 flux. The accumulation chamber method is a static technique which involves the determination of the rate of increase in the CO_2 concentration within an inverted chamber placed on the soil surface. One of the main characteristics of this method has been described by Tonani and Miele (1991) showing that the accumulation chamber is an absolute method that requires neither assumptions nor corrections depending on soil characteristics.

7.2 Instrumentation and analytical procedure

CO_2 flux was measured on site using the accumulation chamber method. The WEST System portable flow meter was used. Figure 7 shows the main components of the flow meter: gas accumulation chamber, pump, a palm top, infrared analyzer LICOR LI-880 and an infrared analyzer WEST TOX-O5-H2S-BH is used for H_2S measurements.

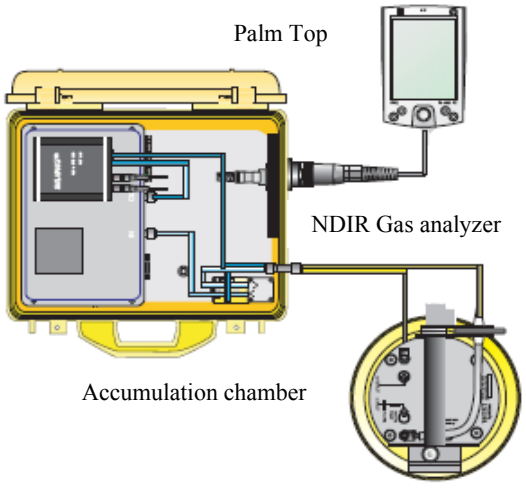

FIGURE 7: Schematic description of LICOR LI-880 Gas Analyzer (Rogie et al., 2007)

7.3 Principle of the method

The LICOR LI-800 Gas Analyzer is an absolute, non-dispersive, infrared (NDIR) gas analyzer based upon a single path, dual wavelength, and infrared detection subsystem. The CO_2 measurement is a function of the absorption of IR energy as it travels through the optical path. Concentration measurements are based on the difference ratio in the infrared absorption between reference and sample signals. Reference and sample channels measure CO_2 in a single path through the use of narrow band optical filters with appropriately selected bands. The CO_2 sample channel uses an optical filter centred at 4.24 µm. This filter corresponds to the absorption band for CO_2. Concentrations of CO_2 present in the optical path will result in a reduction in IR energy. The reference channel is established using a filter with a central wavelength at 3.95 µm. It follows that the out-of-band channel will experience no absorption due to CO_2 and thus serves as a reference since the detector receives the full energy of the source (Rogie et al., 2007).

The instrument uses digital signal processing techniques to determine the temperature and pressure corrected CO_2 concentration based on the optical bench signals through the use of a ratio technique.
The detector responds to thermal energy so it is necessary to precisely regulate the detector temperature. This allows for differentiation of thermal gradient noise from the signals received from the optical path.

Part of the CO_2 concentration calculation depends on the pressure observed in the optical path, measured with an in-line pressure transducer. Many parameters can affect the pressure and thus the concentration reading. The processing centre in the analyzer reads the pressure reading as part of its data collection task and uses this information in the concentration calculation. The gas flow enters the source housing, passes down the optical path and exits at the detector housing. The maximum flow rate for the analyzer is approximately 1 l/min.

Another key parameter in the concentration calculation is the gas temperature in the optical path. It is assumed in the analyzer operation that the gas temperature will equilibrate to the optical bench temperature (50°C) by the time it enters the optical path. Since the instrument performs temperature and pressure corrections as part of the concentration calculation, this assumption is very important.

7.4 Calculation

Gas circulation is maintained through a filter which is responsible for humidity avoidance in the CO_2 detector and is able to measure infrared radiation absorbed by CO_2 gas when passed through a cell at a constant temperature of 50°C. The detector is connected to an accumulation chamber where the soil gas is stored for a known period of time (4 minutes).

Measurement signals are transmitted through an RS232 cable and logged into a PalmTop device using the Palm Flux software. The values obtained are in parts per million per second units (ppm.s^{-1}). These values are the slope of CO_2 concentration vs. time plots ($m = \Delta C/\Delta t$) which are produced every minute (see Figure 8).

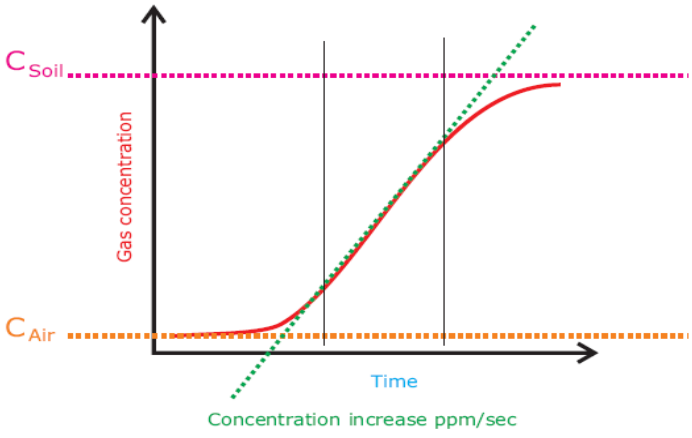

FIGURE 8: Increase in concentration ratio in ppm s^{-1} (from Rogie et al, 2007)

The slope obtained is then used to calculate the CO_2 flux in mol of CO_2 per square meter per day (mol CO_2.day^{-1}.m^{-2}) according to the following procedure:

The first step is to calculate the

accumulation chamber factor (*Kac*) which is dependent on the accumulation chamber dimensions as well as barometric pressure and air temperature. The *Kac* dimensions are mol $m^{-2}d^{-1}ppm^{-1}$ sec.

$$Kac = \frac{864000 \times P}{10^6 \times R \times T} \times \frac{V}{A} \quad (6)$$

where P is the barometric pressure in mbar
R is the gas constant 0.08314510 in bar L/mol K
T is the air temperature in degrees K
V is the volume of the accumulation chamber in m^3 (0.002756 m^3)
A is the area of the accumulation chamber in m^2 (0.03062 m^2)

When the *Kac* value is known, the CO_2 efflux in $mol.m^{-2}.day^{-1}$ is then calculated as the product of the slope ($m = \Delta C/\Delta t$) and the calibration constant:

$$CO_2 \text{ flux } (mol/m^2.day) = m \text{ x } Kc \quad (7)$$

where m is the slope
Kc is the calibration constant

Finally the CO_2 efflux value in $g/m^2.day$ units is calculated multiplying the value in the equation (5) by the molecular weight of CO_2 (44 $g.mol^{-1}$).

The instrument is able to measure CO_2 and H_2S efflux simultaneously through a system with two non-dispersed infrared detectors and one interchangeable measurement cell. This cell is capable of measuring values in the range of 0 to 2,000 parts per million (ppm) and in the range of 0 to 20,000 parts per million (ppm) respectively.

7.5 Methodology

Soil gas flux was determined at 150 stations during the period February 13 and April 11, 2008. Figure 9 shows these locations marked as + symbols. The sites were located at an average separation of 250 m in the E-W direction and in the N-S direction in a total studied area of 10 km^2. Note that the locations were selected to cover the area in a more or less regular grid. Soil pressure gradients and soil temperatures were measured at each flux determination point. Appendix 4 shows the data surveyed.

7.6 Statistical analysis of CO_2 flux data

Cumulative probability plots were suggested by Chiodini et al. (1998) in order to determine partitioning of complex distributions into different normal (or log-normal) populations and the estimation of statistical parameters of each identified population. This graphical statistical analysis is based on the procedure of Sinclair (1974) which consists of a detailed analysis of the distributions in probability plots.

Probability plots as the basis for a statistical analysis have been applied to the results of CO_2 flux in order to separate background populations from anomalous CO_2 flux populations and to compute the total CO_2 output, and relative uncertainties from the different sources in areas surveyed.

The procedure involves approximating segments of a probability curve by straight lines and picking threshold values at ordinate levels that correspond to intersections of these linear segments. At best, this method is approximate, at worst it can result in a high proportion of anomalous values going unrecognized.

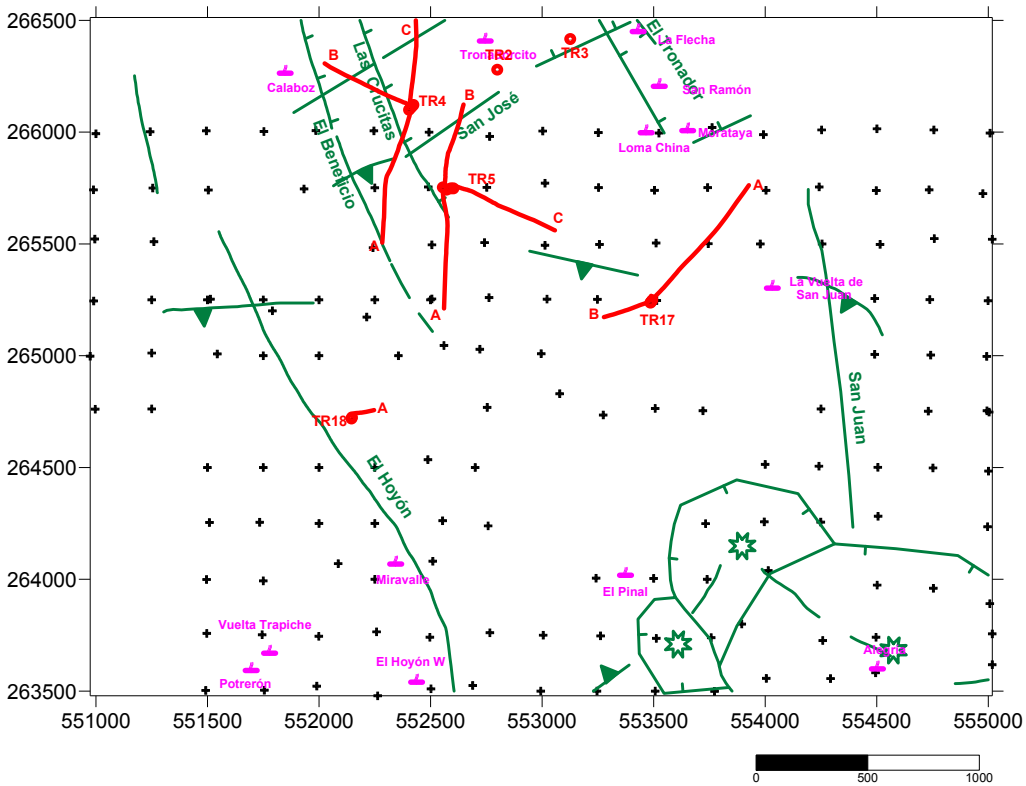

FIGURE 9: Studied area and locations for CO_2 flux measurement. The regular grid with W-E orientation is shown and determination points are represented by a $^{+}$ symbol

A probability graph has on the X-axis a scale of percentages reading from 0.01% on the left to 99.99% on the right. The scale is not evenly spaced; but much more crowed in the middle than at the sides, being specially arranged so that when any normally distributed population is plotted, in a manner which will shortly be described, the points all fall on a straight line. The position of this line is determined by the mean and its slope by the standard deviation. If a bimodal or a polymodal is compounded from distributions which are distributions which are themselves normally distributed, and with geochemical data this is generally true enough for practical purposes, when plotted it will give a curve which is the resultant of two or more straight lines.

If the efflux data are composed of some overlapping normal populations, the plot would have a curve shape with as many inflection points as populations. In the earth sciences it is common for data not to have normal, but lognormal overlapping populations. For this reason, we have to select the logarithmic scale for the efflux data axis.

The log probability graph has been constructed in accordance with the following procedure:

- The first step is ordering the original data in a column from the lowest to the highest value.
- Enumerate the data, i.e. the lowest value is given the number 1, the following the number 2 and so on. The highest value will have the N number, N being the number of total data.
- Once the column has been enumerated, the cumulative proportion of each data is computed according to equation (8)
- Plot the original ordered data versus the cumulative percentage (the column obtained in step 3).

$$\text{Cumulative percentage} = (\text{"Number"} - 0.01)*100/N \quad (8)$$

The cumulative percentage must be plotted with a probability scale. Grapher 6.0 was used for plotting the results. Partitioning is carried out through the examination of a logarithmic probability plot, following the procedure described by Harding (1949), and Sinclair (1974).

Because the computed statistical parameters (i.e., M_i and σ_i) refer to the logarithm of values, the mean value of CO_2 flux (MN_i) and the central 90% confidence interval of the mean, are estimated by means of Sichel´s t-estimator (David, 1977).

7.7 Results

The soil CO_2 fluxes measured are reported in the probability plot shown in Figure 10. The CO_2 fluxes are distributed over a wide range of values (Table 9) and plot along a line if one neglects slight divergences at the extremities.

In this case, the range of values and the form of the probability graph suggest that the data represent a single background population with the exception of upper values. A wise procedure is to assume that the few highest values are anomalous until proven otherwise (Sinclair, 1974).

This is a convenient safety precaution in cases where anomalous values are present in too low a proportion to define a second population selecting an arbitrary threshold at an ordinate level corresponding to the mean plus 2 standard deviations (Hawkes and Webb, 1962). This procedure assumes that approximately the upper 2.5% of values are anomalous until shown otherwise, and should be applied only when a single population is indicated from an examination of the probability graph.

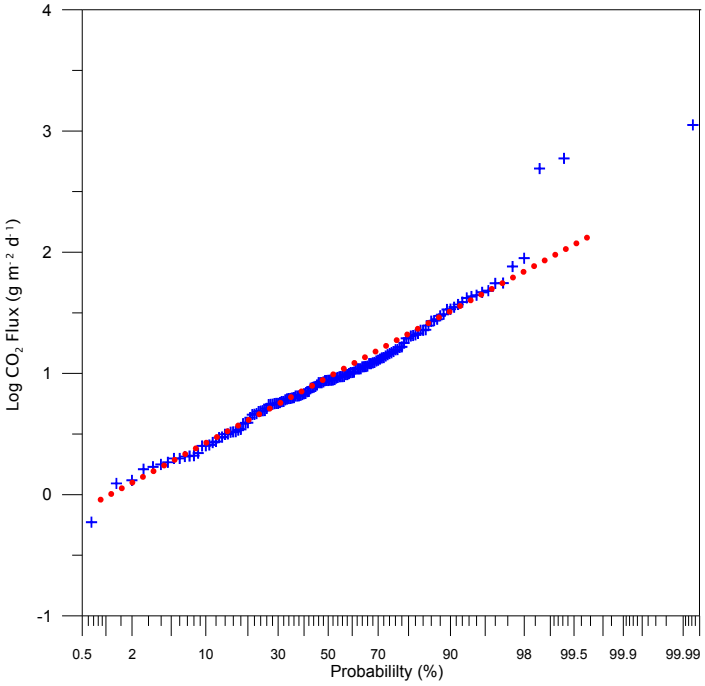

FIGURE 10: Logarithmic probability plot of CO_2 flux through soil in the southern region of the Berlin geothermal field

TABLE 9: Statistical parameters of the measured CO_2 flux at the Berlin southern region

No. of measurements	Min. CO_2 flux (g m^{-2} d^{-1})	Max. CO_2 flux (g m^{-2} d^{-1})	Average CO_2 flux (g m^{-2} d^{-1})
150	0.593	1121.7	38.021

Two considerations confirm that the previously mentioned assumption is valid. Firstly, the 2.5% of 150 sampled points correspond to 4 anomalous values which are located in areas where the convergence of faults, craters and caldera borders take place; those are areas of hydrothermal activity such as the Laguna de Alegria, El Pinal and El Hoyón fumaroles where a high steam ratio has been reported by CEL (1991) and (Lageo, 2004). Secondly, soil CO_2 flux values ranged between 89.34 and 1121.17 g m^{-2} d^{-1} and represent high fluxes considering that soil CO_2 flux values of up to several tens of g m^{-2} d^{-1}, are associated with a biogenic background source, whereas higher CO_2 fluxes (up to 10^3 – 10^4 g m^{-2} d^{-1}) are considered to be representative of the volcanic-hydrothermal source (Chiodini et al., 2008).

Two previous studies have been aimed at determining the CO_2 discharge from the Berlin geothermal system. Magaña and Guevara (2001) and Lopez et al. (2004b) studied the CO_2 efflux in the northern region of the Berlin system determining values in the range of 0-500 g m^{-2} d^{-1} and 0-2000 g m^{-2} d^{-1} respectively. Differences in values should be noted and related to zones of hydrothermal alteration that have been included by Lopez et al. (2004b). Higher values of CO_2 efflux are found in the advective zones suggesting a relationship with the main fault system in the region, the NW-SE and the NNE-SSW fault systems. Results of these investigations suggested that the occurrence of

hydrothermal manifestations, the release of hot gases and vapour, and the transfer of heat, are coupled processes that are related to the fault systems in the area (Magaña et al., 2003 and 2004).

Despite the evidences of the volcanic-hydrothermal source for these anomalous samples, statistical analysis cannot be conducted for the reduced amount of samples and the estimated mean flux values have been used to compute the total CO_2 output associated with the data population obtained assuming one single population. Table 10 summarizes estimated parameters of the population studied and diffuse CO_2 output.

The total CO_2 output from the entire study area is then estimated by multiplying the total surface area (*S)* with the mean value of CO_2 flux (*MN*). Similarly, the central 90% confidence interval of the mean is used to calculate the uncertainty of the total CO_2 output estimation of the population. The total CO_2 output from the area surveyed (F_{CO}) is equal to 17593 t y^{-1} with 23105 and 14162 t y^{-1} as the maximum and minimum values, respectively, estimated from the confidence limits (σ).

TABLE 10: Estimated parameters and diffuse CO_2 output

***f* (%)**	***M* ± σ**	***MN* (g m^{-2} d^{-1})**	***S* (m^2)**	**F_{CO} (t d^{-1})**
100	0.97 ± 0.48	4.82 (6.33-3.88)	10 x 10^6	48.2(63.3– 38.8)

8. TOTAL CARBON MEASUREMENTS

8.1 Theoretical aspects

The study of CO_2 fixation in calcite in the southern region of the high temperature Berlin geothermal field is facilitated by a number of geothermal wells that have been drilled recently. Drill cuttings, collected at uniformly spaced intervals throughout the entire depth of the wells, allow detailed studies of the amount of CO_2 that is fixed in the rocks.

Carbon dioxide content was measured in 50 samples of drill cuttings from 5 wells in the southern production zone of the field. The data obtained was used to estimate the total amount of CO_2 fixed in rocks in this system over the geothermal system's lifetime. By comparing these results to observed atmospheric emissions of CO_2 from this system, the relative importance of these of these two geothermal sinks for geothermal CO_2 is recorded.

The carbon dioxide content obtained from laboratory analysis of drill cuttings samples was used to estimate vertical distribution patterns in the area studied; the vertical variation of the amount of fixed CO_2 is then used to compute the mass of CO_2 in the uppermost 1500 m of the bedrock, per unit surface area.

TABLE 11: Measured depth of samples (in m) for total carbon analyses

TR-17	TR-17A	TR-17B	TR-18	TR-18A
320	100	160	250	100
410	250	315	480	200
600	500	410	750	245
820	780	500	995	340
1000	1055	600	1205	520
1200	1200	700	1290	605
1395	1780	845	1400	680
1500	2110	1100	1845	735
2000	2457	1150	2600	800
2417	2628	1250		900

8.2 Sampling

Table 11 shows samples used for carbon analysis. Selection of samples was made keeping uniformly spaced intervals along the well depth as well as availability of samples due to circulation loss during well drilling.

8.3 Analytical technique for total carbon measurements

About 5 g of drill cuttings were ground to a fine powder using a carbide ball mill. The pulverized rock samples were combusted in oxygen in a CM5200 Auto sampler Furnace from UIC Inc. Coulometrics. The total carbon in the CO_2-containing gas stream was determined with an UIC Inc. Model 5014 CO_2 Coulometer.

A known mass of about 20 mg from each sample taken from the 5 g of pulverized rock is combusted in oxygen at 950°C to convert all carbon to CO_2. The sample combustion gases are swept through a barium chromate scrubber to ensure complete oxidation of carbon to CO_2. Non-carbon combustion products are removed from the gas stream by a series of chemical scrubbers. The CO_2 is then measured with the CO_2 coulometer. The coulometer cell is filled with an appropriate solution containing monoethanolamine and a colorimetric pH indicator. Platinum (cathode) and silver (anode) electrodes are positioned in the cell, which is then placed in the coulometer cell compartment between a light source and a photometric detector in the coulometer.

As a CO_2 gas stream passes into the cell, the CO_2 is quantitatively absorbed, reacting with the monoethanolamine to form a titratable acid. This acid causes the colour indicator to fade. Photo detection monitors the change in the colour of the solution as a percent transmittance (%T). As the %T increases, the titration current is automatically activated to electrochemically generate base at a rate proportional to the %T (approximately 1500 µg carbon/minute). When the solution returns to its original colour (original %T), the current is terminated. The coulometer is based on the principles of

Faraday´s Law. Each faraday of electricity expended is equivalent to 1 GEW (gram equivalent weight) of CO_2 titrated, which is important for calibration. By knowing the total weight of the sample and the weight of carbon contained therein, the weight percentage of carbon can be calculated.

A summary of the chemical reactions taking place in the coulometer cell is shown:

i) Absorption of CO_2 by cathode solution (cathode reaction)

$$CO_2 + HOCH_2CH_2NH_2 \rightarrow HOCH_2CH_2NHCOOH \quad (9)$$

monoetanolamine hydroxyethylcarbamic acid

ii) Electrochemical generation of OH^- (cathode reaction)

$$2\ H_2O + 2e- \rightarrow H_2\ (g) + 2OH- \quad (10)$$

iii) Neutralization of absorbed CO_2 reaction product by electrochemically generated OH^-

$$HOCH_2CH_2NHCOOH + OH^- \rightarrow HOCH_2CH_2NHCOO^- + H_2O \quad (11)$$

iv) Anode reaction

$$Ag^o \rightarrow Ag^+ + e- \quad (12)$$

A calcite standard of 99.9% purity was used to verify the accuracy and precision of the measurements. Based on the ratio of the molecular weight of carbon (12.011 g/mol) and calcite (100.0892 g/mol), 99.9% calcite is equivalent to 11.99% carbon. The arithmetic mean of 3 readings was 11.4417% with a standard deviation of 0.06. (see Table 12). The accuracy of the instrument is acceptable for the purpose of the carbon measurements presented in this study.

TABLE 12: Results of standard analyses

Calcite (wt%)	Carbon (wt%)	Number of readings	Arithmetic mean (wt%)	Standard deviation (wt%)
99.9	11.99	7	11.47	0.06

8.3.1 Background carbon

CO_2 may be present in the rock before the beginning of the accumulation of geothermal calcite. It is, therefore, necessary to evaluate the initial CO_2 content of the unaltered andesites. Not all magmatic CO_2 is released during cooling and crystallization of the andesites; some of it may be present in fluid inclusions in crystals as well as trapped in undegassed glass after cooling. In order to provide an estimate of the CO_2 content of unaltered andesites, a sample from well TR-17A at a depth of 100 m was used for background correction; this sample was selected based on alteration mineralogy analysis where andesite is formed by a 4% of alteration minerals (LaGeo, 2008a). The arithmetic mean of three readings was 0.012% C with a standard deviation of 0.001.

8.3.2 Data treatment

Carbon percentage was determined in duplicate in drill cutting samples and an arithmetic mean value has been reported in Appendix 5. In any case, the relative error never exceeds 17.72% which is acceptable for the purpose of this study. In addition, background carbon was subtracted from the arithmetic mean value, next the weight percentage of carbon was converted to weight percentage of CO_2 and then into tons of CO_2 per unit volume of rock by multiplying by the density of the andesite. The average density value from core samples for the wells studied reported by Lageo (2008a) is 2,600 kg/m^3. A correction factor of 1.04 was applied in order to avoid calcite affecting the bulk density.

The density of calcite is equal to 2700 kg/m^3 (Deer et al., 1992). The concentration of CO_2 in the rock is computed by

$$CO_2 \text{ (kg/m}^3\text{)} = CO_2 \text{ (wt\%)} / 100 * 2{,}600 \text{ kg/m}^3 * 1.04 \quad (13)$$

8.4 Results

8.4.1 Vertical distribution patterns

The amounts of CO_2 as a function of depth from wells studied in the southern region of the Berlin geothermal field are shown in Figures 11-15. The values for fixed CO_2 range between 0.0 kg/m^3 and 194.0 kg/m^3. Both extreme values were observed in well TR-17A, at 980 and 830 m a.s.l. respectively.

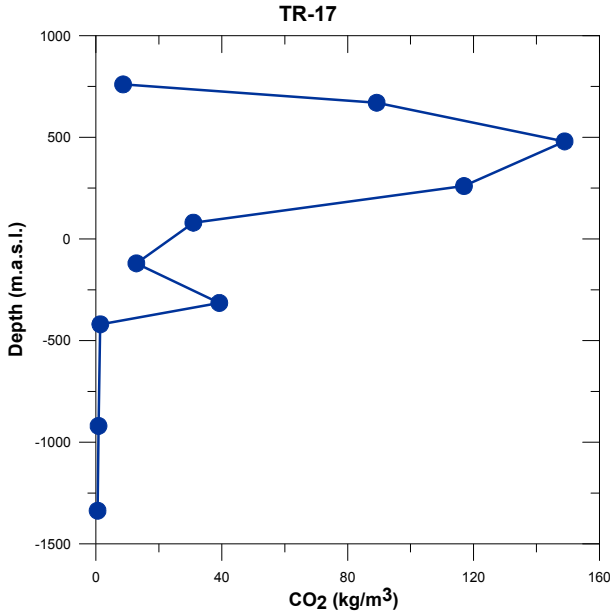

FIGURE 11: CO_2-depth profile for well TR-17

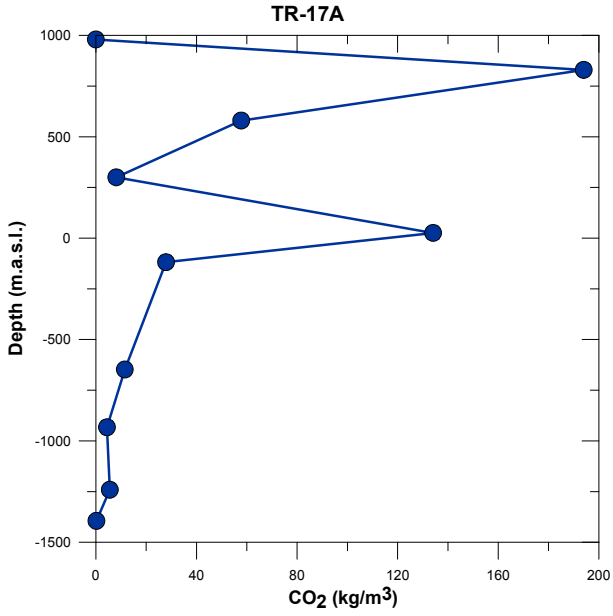

FIGURE 12: CO_2-depth profile for well TR-17A

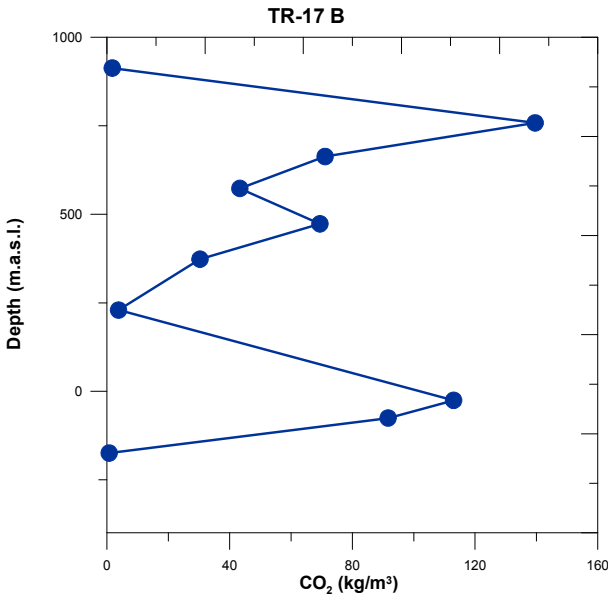

FIGURE 13: CO_2-depth profile for well TR-17B

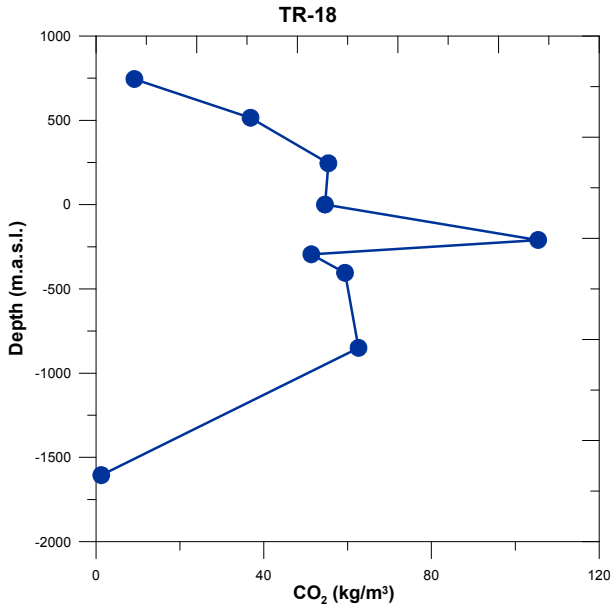

FIGURE 14: CO_2-depth profile for well TR-18

Wells TR-17, TR-17A and TR-17 B were drilled from the same platform; the former is a vertical borehole with a total depth of 2600 m; well TR-17A is a directional well with a final depth of 2690 m and total vertical displacement (TVD) of 2530.17 m with N 45° E direction; the latter, is a directional one and is shallowest with a total depth of 1845 m and TVD of 1809 with N254° direction. Wells TR-18 and TR-18A share the same platform, the former is a vertical well with 2660 depth and the latter is a directional well with total depth of 1085 m and TVD of 1072 m oriented N 71° E.

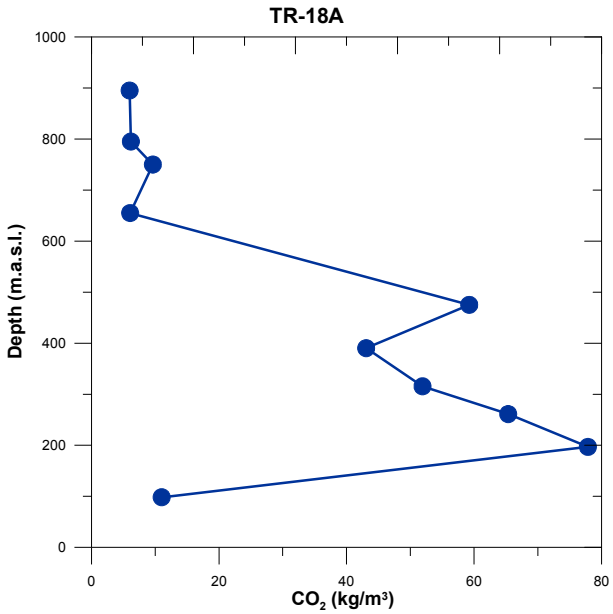

FIGURE 15: CO_2-depth profile for well TR-18A

The highest amount of fixed CO_2 in well TR-17 is found at 480 meters depth; then the values of Captured CO_2 in kg/m^3 start decreasing up to 1200 meters depth and then increase up to 39 kg/m^3 at 1395 depth. At higher depths the pattern of fixed CO_2 show values lower than 1.39 kg/m^3. For this well, the highest CO_2 fixation occurs between 410 and 1395 meters depth.

A similar pattern can be observed in well TR-17A where CO_2 fixation occurs between 250 and 1200 meters depth; then captured CO_2 values start decreasing down to the bottom of the well. From the five wells studied, the highest amount of fixed CO_2 was computed as 194 kg/m^3 at 250 m depth. One additional particularity for this well is the fact that this high value is found at the shallowest depth.

Well TR-17B shows relatively high CO_2 values down the borehole with the exception of samples from 160, 845 and 1250 m depths. Drill cuttings samples were analyzed up to 1250 meters depth (-177 m a.s.l.) because deeper samples were not available due to total loss of circulation during the drilling of the borehole; for this reason is not possible to confirm the observed pattern below this depth as the previous wells in.

For wells TR-17 A and TR-17 B, it is noted that at a depth between 26 and -26 m a.s.l., the amount of CO_2 fixed shows considerably high values of 134 and 113 kg/m^3 respectively. No sample was collected in well TR-17 at that depth but the samples collected close to the previously mentioned depth range seems to show values in agreement with the rest of the wells on this platform.

Captured CO_2 in wells TR-18 and TR-18A seems to be lower in magnitude than in wells TR-17, A and B. The highest amount was found in well TR-18 at 1205 m depth which value corresponds to 105.45 kg/m^3. Apart from this point, the amount of CO_2 fixed in well TR-18, ranged between 36.84 and 62.60 kg/m^3 with the exception of the shallower sample at 250 m depth where the computed value was 9.14 kg/m^3 and the deeper sample collected at 2600 where the computed value was 1.24 kg/m^3.

The pattern for well TR-18 differs significantly from those in the previously described wells in two aspects. Firstly, the fixed CO_2 appears in significant amounts up to 1845 m depth (-1250 m a.s.l.). Secondly, CO_2 fixation starts to be significant at greater depths than in wells TR-17, at 480 m depth the amount of CO_2 fixed is 59.24 kg/m^3. This deep CO_2 fixation could be explained with reference to fluid inclusion temperatures (Lageo, 2008a). Despite the fact that wells on the platform of TR-17 show lower temperatures than those reported for wells on the platform of TR-18; fluid inclusions studied from well TR-18 in core samples at 1053-1057, 2050-2055, and 2600-2603 m depth revealed that calcite temperature ranged between 195-240, 268-277, and 249-267 °C respectively at these depths. These temperatures are lower than the homogenization temperatures reported for wells TR-17 and 17A which ranged between 272 and 305°C. In all cases, higher temperatures have been reported between 2000-2100 m depth.

Well TR-18A shows the lowest computed values for fixed CO_2 of all the wells studied. The highest values were found at 800 m depth and the pattern seems to be uniform between 500 and 800 m depth. As was described for well TR-18, the amount of CO_2 fixed becomes significant at 500 m depth. A considerable reduction can be observed at 900 m depth. Due to lack of samples at greater depths, confirmation of the well TR-18A pattern beyond 900 m depth was not possible.

8.4.2 Spatial distribution

Figure 16 shows the vertical variation of the amount of fixed CO_2 with depth. A NE-SW cross section was plotted intersecting wells TR-17 and TR-18. Map Info software was used to plot the cross section and the minimum curvature gridding method was used to interpolate between wells. The colours indicate the mass of fixed CO_2 in kg/m^3.

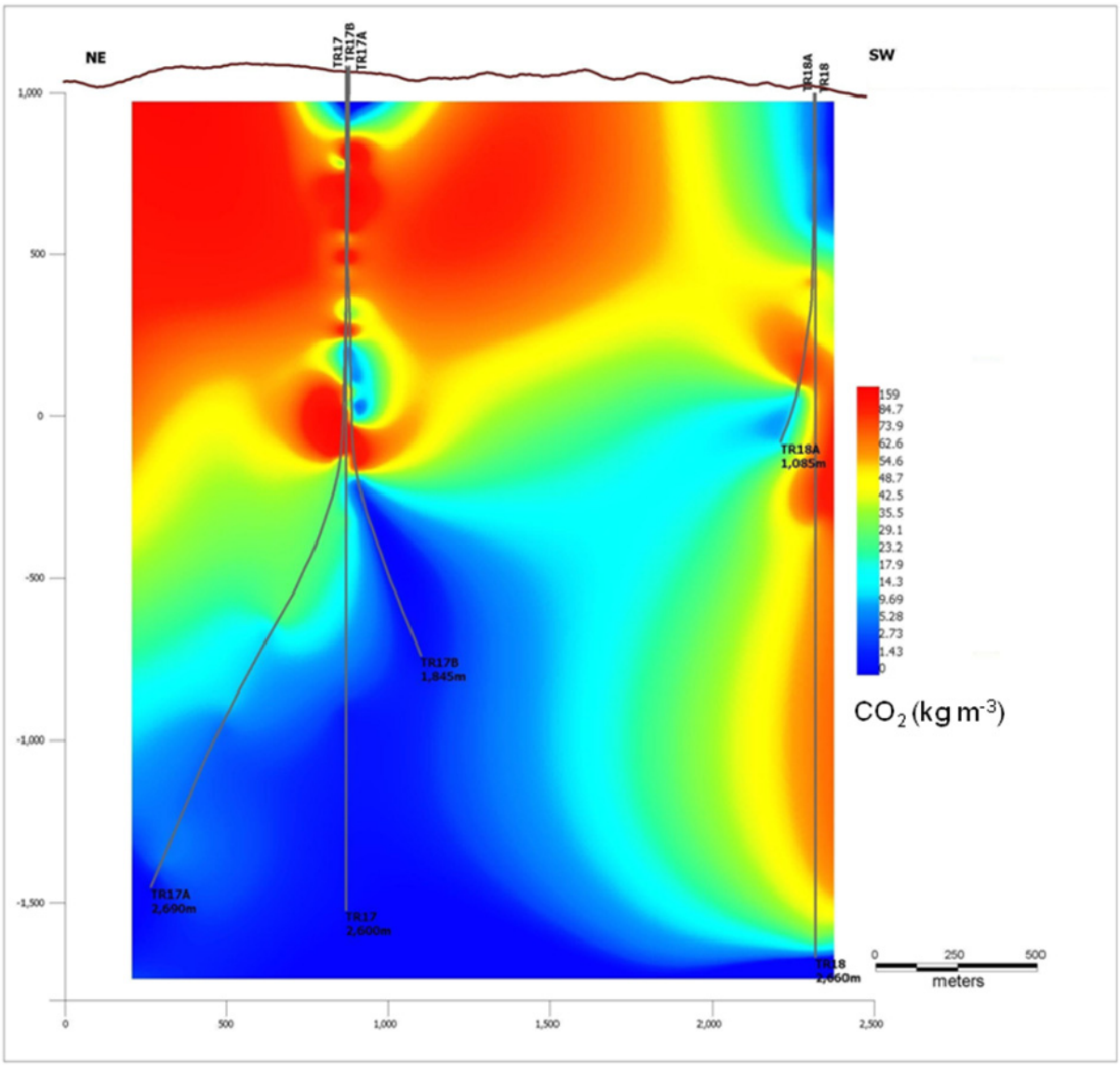

FIGURE 16: NE- SW cross section depicting the distribution of CO_2 fixed in the bedrock at Berlin

The inset map (Figure 17) shows the location of wells drilled in the Berlin geothermal field.

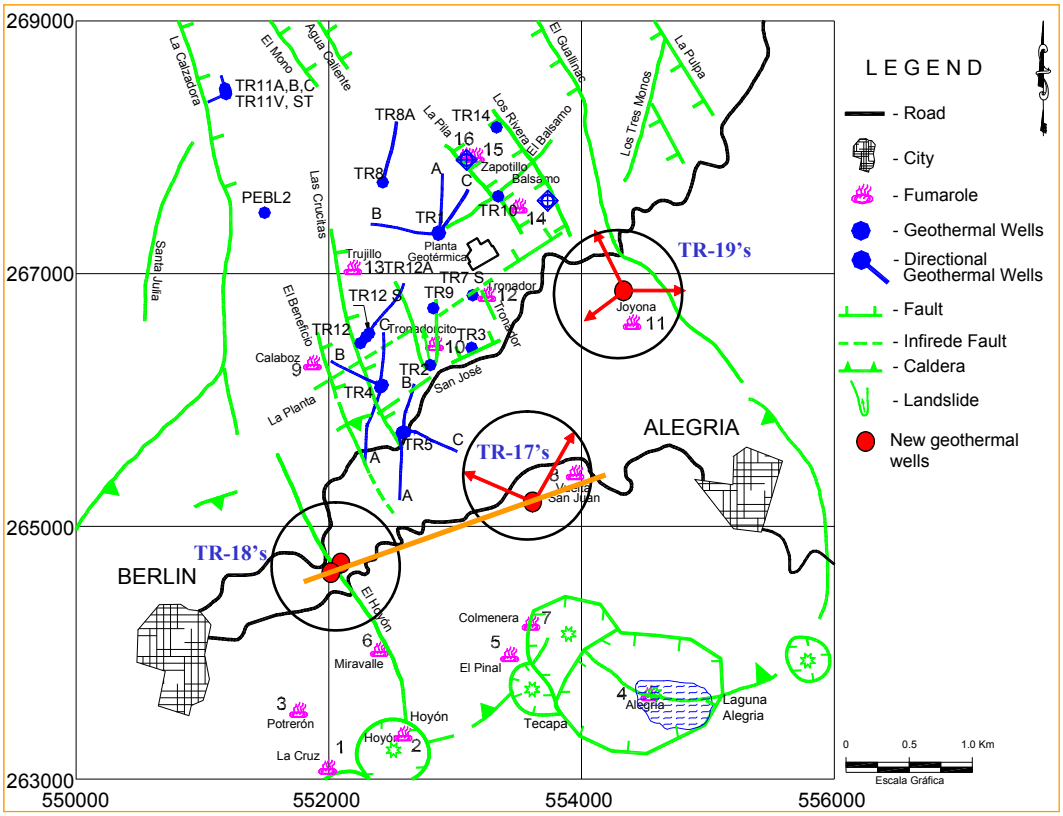

FIGURE 17: Location of wells drilled in the Berlin geothermal field, red and blue dots depict vertical wells and red and blue lines depict directional wells; the orange line describes the orientation of the NE-SW cross section

From what has been described it seems clear that an overall pattern of calcite distribution for the wells studied is not well defined, for wells TR-17 the abundance increases with depth until it reaches a maximum value at about 250 to 600 m depth and then decreases gradually with increasing depth, then a low CO_2 fixed region can be noted between 300 and -10 m a.s.l. with SW orientation. At lower depths starting at 1200 m depth, a reduction in the CO_2 fixed can be observed. The region with low fixed CO_2 values western well TR-17B is explained by the lack of samples at that depth but it seems to describe a similar pattern to the one observed for the rest of the wells at that depth. For wells TR-18 and TR-18A CO_2 fixed in the bedrock becomes significant at 500 m a.s.l., with a reduction pattern to the NE at elevation lower than - 300 m a.s.l.

8.4.3 Mass of CO_2 fixed in the bedrock per unit surface area

The mass of CO_2 per unit surface area in the uppermost 1500 m of the bedrock was computed from the observed CO_2 concentration profiles for the five wells studied in the southern region of the Berlin geothermal field. This value is a meaningful estimate of the amount of geothermal CO_2 fixed in the bedrock because almost all CO_2 has accumulated above 1500 m in these systems.

The CO_2 load of individual wells was computed by finite elements integration (Wiese et al., 2008). The CO_2-depth profile for a given well was divided into segments so that each CO_2 value was in the middle of each segment. The total CO_2 fixed in the uppermost 1500 m of the crust was found by summing up the products of the length of each segment (in m) by the measured CO_2 concentration at the center of that segment (in kg/m^3). The resulting value is expressed in the units kg/m^2 or the more convenient t/m^2.

The computed CO_2 load of the uppermost 1500 m of the crust for individual wells and the average value are shown in Table 13 below.

Computed values for the Berlin geothermal system could be enhanced including information from a representative number of previously drilled wells in the northern part of the system. The CO_2 load of 79.5 t/m^2 is based on 13% of the total number of wells. However, the computed values based on the five studied wells, seem to be representative of the geothermal system as a whole.

TABLE 13: CO_2 load in the uppermost 1500 m of studied wells

Well	CO_2 load (t/m^2)
TR-17	83.45
TR-17 A	101.08
TR- 17 B	64.12
TR-18	106.96
TR-18 A	41.74
Average	**79.5**

8.5 Total mass of fixed CO_2

The total amount of CO_2 fixed in the studied area can be roughly estimated by multiplying the average CO_2-load of the wells in a given system by its areal extent. Monterrosa (2002) has estimated the possible extended area of the Berlin system as 10 km^2.

The total amount of CO_2 fixed in the Berlin geothermal system has been amounted to 795 Mt. As an approximation of the total amount of CO_2 fixed in calcite crust, it has been assumed that the estimated amount for Berlin is representative of the high temperature geothermal systems in El Salvador. Ten High temperature geothermal systems have been identified in El Salvador, with an approximate surface of 36 km^2 (Campos, 1981). Based on the assumption that the total CO_2 content of the Berlin is representative, the total CO_2 fixed in active high-temperature geothermal systems in El Salvador, this amounts to 2.5 – 3.5 Gt of CO_2.

8.6 Calcite fixation and the CO_2 budget of the Berlin geothermal systems

The age of the Berlin geothermal system has been estimated as10 to 130 ky (GENZL, 1995). This age is used together with the approximate areal extent and the average CO_2-load of the crust of the Berlin geothermal system to evaluate the time it has taken the calcite to accumulate. The estimated CO_2 fixation rate of calcite is 6100 to 79500 t y^{-1} (0.61 – 7.95 kg m^{-2} y^{-1}).

Table 14 shows the computed values as well as date published by Fridriksson et al. (2006), Ármannsson et al. (2007) and Wiese et al. (2008) from the Krafla and Reykjanes geothermal systems in Iceland. Computed CO_2 fixation rate values for the Berlin geothermal system almost doubled the computed values for Reykjanes. On the other hand, computed CO_2 emissions from Berlín are lower than those computed for Icelandic geothermal systems.

TABLE 14: CO_2 fixation rates and natural atmospheric emissions in geothermal systems

Geothermal System	Area (km^2)	Fixed CO_2 (kg/m^2)	Age (Ma)	Fixation rate (kg/m^{2}y)	CO_2 emissions (kg/m^{2}y)
Berlín	10	79500	0.01 – 0.13	0.6 – 7.9	1.76
Reykjanes	2	28200	0.01 – 0.10	0.3 – 2.8	2.5
Krafla	30	73100	0.11 – 0.29	0.3 – 0.7	4.25

9. CONCLUDING REMARKS

Two geochemical sinks for CO_2 in geothermal systems, have been successfully studied as the first attempt to understand the CO_2 budget of the Berlin geothermal system and its implications for the evaluation of the environmental impact through the CO_2 emissions of the power generation caused by the emissions of CO_2 to the atmosphere.

The total carbon dioxide emission rate from the Berlin geothermal power plant amounted to 42420 t y^{-1} in the year 2008. This value is 2.4 times higher than those computed from natural CO_2 soil degassing in the studied area in the same period. Computed emissions from the Berlin power plant in terms of g kWh^{-1} of net electricity generation, are significantly lower than those from power stations using fossil fuels but are significant compared to natural emissions through soil in the Berlin geothermal system.

The amount of CO_2 fixed in the southern region of the Berlin geothermal field computed in the present study is 795 Mt which is about 92 times the annual anthropogenic CO_2 emissions of El Salvador estimated as 8.6 Mt (PNUMA, 2007).

The CO_2 fixation and natural atmospheric emission rates in the Berlin geothermal system could be improved if steam vent discharge and gas bubbling through steam heated pools are included in further work. Several investigations have demonstrated that in geothermal systems, most of the CO_2 is emitted from the magma to the atmosphere through soil diffuse degassing. Assuming that all natural CO_2 emissions are transported through the soil, the accumulated CO_2 emission rate would be no less than 1.76 kg m^{-2} y^{-1} which is comparable with the CO_2 fixation estimated in the present study.

No attempt has been made to evaluate the amount of CO_2 dissolved in enveloping groundwater of Berlin. It is of relevant importance to address this component of the CO_2 budget of geothermal systems in further studies. Atmospheric emissions through steam vents are also needed to be completed.

REFERENCES

Arias, A., Bertani, R. Ceccarelli, A., Dini I., Fiordelisi, A. Marocco B.M., Scandiffio G., Volpi, G. Barrios, L. Handal, S., Monterrosa, M. Quezada A., and Santos, P., 2003: Conceptual Model review of the Berlín geothermal system. *Geothermal Resources Council, Transactions*, *27*, 755-759.

Ármannsson, H., 2003: CO_2 emission from geothermal plants. *Proceedings International Geothermal Conference, Reykjavík*, *September, 2003*, 56-62.

Ármannsson H., Fridriksson, Th., and Kristjánsson, B., 2005: CO_2 emissions from geothermal power plants and natural geothermal activity in Iceland. *Geothermics 34*, 286-296.

Ármannsson, H., Fridriksson, Th., Wiese, F., Hernández, P., and Pérez, N., 2007: CO_2 budget of the Krafla geothermal system, NE-Iceland. In: (Eds.) Bullen, T.D., and Yangxin W. *Proceedings of the 12th International Symposium on Water-Rock Interactions*, *WRI-12, Kunming, China, 31 July – 5 August. 2007*, 189–192.

Arnórsson, S., and Gíslason, S.R., 1994: CO_2 from magmatic sources in Iceland. *Min. Mag., 58A*, 27-28.

Arnórsson, S., and Gunnlaugsson, E., 1985: New gas geothermometers for geothermal exploration – calibration and application. *Geochim. Cosmochim. Acta, 49*, 1307-1325.

Arnórsson, S., D´Amore, F., and Gerardo Abaya, J., 2000: Isotopic and chemical techniques in geothermal exploration, development and use. In: Arnórsson, S. (ed.). *Isotopic and chemical techniques in geothermal exploration, development and use: Sampling methods, data handling, interpretation*. International Atomic Energy Agency, Vienna, p. 317.

Arnórsson, S., Sigurdsson, S., and Svavarsson, H., 1982: The chemistry of geothermal waters in Iceland I. Calculation of aqueous speciation from 0°C to 370°C. *Geochim. Cosmochim. Acta*, 46, 1513-1532.

Arnórsson, S., Stefánsson, A., and Bjarnason, J., 2007: Fluid-fluid interaction in geothermal systems. *Reviews in Mineralogy and Geochemistry*, *65*, 259-312.

Bertani, R., and Thain, I., 2002: Geothermal power generating plant CO_2 emission survey. *IGA news 49*, 1-3.

Bjarnason, J.Ö., 1994: *Computer code WATCH, version 2.1.* Orkustofnun, Reykjavík, 56 pp.

Campos, T., 1981: *The geothermal resources of El Salvador: Characteristics and preliminary assessment.* CEL, Internal report, 22 pp.

CEL, 1987: *Texture properties of the rocks of the Berlin geothermal field: Porosity, density and permeability*. Internal report (in Spanish).

CEL, 1991: *Summary of geochemistry of the Berlin geothermal system*. Internal report (in Spanish).

CEL, 1996: *Conceptual model of the Berlin geothermal field: Geoscientific information synthesis*. Internal report (in Spanish).

Chiodini, G., Caliro, S., Cardellini, C., Avino, R., Granieri, D., and Schmidt, A., 2008: Carbon isotopic composition of soil CO_2 efflux, a powerful method to discriminate different sources feeding soil CO_2 degassing in volcanic-hydrothermal areas. *Earth and Planetary Science Letters, 274*, 372-379.

Chiodini, G., Cioni, R., Guidi, M., Raco, B., and Marini, L., 1998: Soil CO_2 flux measurements in volcanic and geothermal areas. *Applied Geochemistry*, *13, 5*, 543-552.

D´Amore, F., and Mejia, J., 1998: Chemical and physical reservoir parameters at initial conditions in Berlin geothermal field El Salvador: A first assessment. *Geothermics, 28*, 45-73.

D'Amore, F., and Tenorio, J., 1999: Chemical and physical reservoir parameters at initial conditions in Berlín geothermal field, El Salvador: A first assessment. *Geothermics, 28*, 45-73.

D´Amore, F., and Truesdell, A.H., 1985: Calculations of geothermal reservoir temperatures and steam fractions from gas compositions. *Geothermal Resources Council Transactions, 9*, 305-310.

David, M., 1977: *Geostatistical ore reserve estimation*. Elsevier Scientific Publishing Company, Amsterdam, 364 pp..

Deer W.A., Howie, R.A., and Zussman, J., 1992: *An introduction to the rock-forming minerals* (2^{nd} edition). Pearson Education, 712 pp.

Delgado, H., Piedad-Sánchez, N., Galvian, L., Julio, P., Alvarez, J.M., and Cárdenas, L., 1998: CO_2 flux measurements at Popocatépetl volcano: II. Magnitude of emissions and significance. *EOS Trans., AGU 79,45, F926*.

Electroconsult Spa, 1994: *Feasibility study for the Berlín geothermal field, resource assessment*. Internal Report, (in Spanish).

Ellis, A.J., and Mahon, W.A.J., 1977: *Chemistry and geothermal systems*. Academic Press, New York, 392 pp.

Fridriksson, Th., Kristjánsson, B., Ármannsson, H., Margrétardóttir, E., Ólafsdóttir, S., and Chiodini, G., 2006: CO_2 emissions and heat flow through soil, fumaroles and steam heated mud pool at the Reykjanes geothermal area, SW Iceland. *Applied Geochemistry, 21*, 1551-1569.

GENZL, 1995: Berlin Geothermal Field: *Geovolcanology, geochemistry, scaling and corrosion study*. Internal report (in Spanish).

GESAL, 2001: *Updated conceptual model of the Berlin geothermal field. Lageo S.A. de C.V.*, internal report (in Spanish), 19 pp.

Giggenbach, W.F., and Goguel, R.L., 1989: *Collection and Analysis of Geothermal and Volcanic Water and Gas Discharges.* Unpublished DSIR (New Zealand), report No. 2401.

Harding J.P., 1949: The use of probability paper for the graphical analysis of polymodal frequency distributions. *J. Mar. Biol. Assoc. UK., 28*, 141-153.

Hawkes, H.E., and Webb, J.S., 1962: *Geochemistry in mineral exploration*. Harper and Row, New York, 415 pp.

Hunt, T.M., 2000: *Five lectures on environmental effects of geothermal utilization*. United Nations University Geothermal Training Programme, Report 1, 109 pp.

Lageo, 2004: *Feasibility study for the optimization and development of Ahuachapán, Chipilapa and Cuyanausul geothermal systems: Report on Ahuachapán-Chipilapa. Conceptual model and drilling proposals.* Internal Report, 194 pp.

Lageo, 2007: *Generation report*, *December 2007*. Lageo S.A. de C.V., Internal report (in Spanish), 3 pp.

Lageo, 2008a: *Updated geological conceptual model of the Berlín geothermal field, June 2008*. Lageo S.A. de C.V., Internal report (in Spanish), 17 pp.

Lageo, 2008b: *Generation report, December 2008*. Lageo S.A. de C.V., Internal report (in Spanish), 3 pp.

Lageo, 2009: *Geothermal well logging report during the overhaul of the Unit III in the Berlin geothermal field*. LaGeo S.A. de C.V., Internal report (in Spanish), 17 pp.

Lopez, D., Ransom, L. Pérez, N., Hernandez, P., and Monterrosa, J., 2004a: Dynamics of diffuse degassing at Ilopango Caldera, El Salvador. In: (Eds.) Rose, W.I., Bommer, J.J., López, D.L., Carr, M.J., and Major, J.J. Natural hazards in El Salvador. *Geological Society of America Special Paper, 375,* 191-202.

López, D.L., Padrón, E., Magaña, M.I., Gomez, L., Barrios, L., Pérez, N., and Hernandez, P., 2004b: Structural control on thermal anomalies and diffuse surficial degassing at Berlín geothermal field, El Salvador. *Geothermal Resources Council Transactions, 28,* 477-483.

Lovelock, B.G., 2001: Steam flow measurement using alcohol tracers. *Geothermics, 30*, 6, 641-654.

Lovelock, B.G., and Stowell, A., 2000: Mass flow measurement by alcohol tracer dilution. *Proceedings of the 2000 World Geothermal Congress, Japan*, 2701-2706.

Magaña, M.I., and Guevara, W., 2001: *Complementary diffusive degassing study in the drilling proposals areas in the Berlin geothermal field*. GESAL, internal report (in Spanish).

Magaña, M.I., Henríquez, E., and López, D.L., 2003: Study on diffuse degassing and alteration mineralogy in the Berlín Geothermal Field. *Proceedings of the International Geothermal Conference, Reykjavík, September, 200*, 33-39.

Magaña, M.I.,López, D.L., Barrios, L., Pérez, N., Padrón, E., and Henríquez, H., 2004: Diffuse and convective degassing of soil gases and heat at the TR-6-Zapotillo hydrothermal discharge zone, Berlín geothermal field, El Salvador. *Geothermal Resources Council Transactions, 28,* 485-488.

Molnar, P., and Sykes, L., 1969: Tectonics of the Caribbean and Middle America regions from focal mechanisms and seismicity. *Geological Society of America Bulletin, 80*, *9*, 16-1684.

Monterrosa, M.E., 2002: Reservoir modelling for the Berlin geothermal field, El Salvador. *Proceedings of the 27th Stanford Workshop, 28-30 January 2002*, 406-410.

Mörner, N., and Etiope, G., 2002: Carbon degassing from the lithosphere. *Global and Planetary Change 33*, 185-203.

Nicholson, K., 1993: *Geothermal fluids: chemistry and exploitation techniques*. Springer-Verlag, Berlín, 263 pp.

Pang, Z., and Ármannsson, H., 2006: *Analytical procedures and quality assurance for geothermal water chemistry.* UNU-GTP, Iceland, Report 1, 172 pp.

PNUMA, 2007: *Report of the state of environment in El Salvador 2003-2006*. Environment and Natural Resources Ministry, El Salvador (in Spanish), 176 pp.

Rodríguez, J.A., and Monterrosa, M., 2007: Phased development at Ahuachapán and Berlín geothermal fields. In: Rodríguez, J.A. *Lectures on geothermal in Central America*. United Nations University Geothermal Training Program, Report 1. 7-20.

Rogie, J.D., Kerrick, D., and Chiodini, G., 2007: *Portable diffuse flux meter, carbon dioxide, methane and hydrogen sulphide*, release 7.0. West Systems 2007 website: http://www.westsystems.com/doc/HandBook_LI820_7_0.pdf

Ruggieri, G., Chiara, M.P., Gianelli G., Arias A., and Henriquez E., 2006: Hydrothermal alteration in the Berlin geothermal field (El Salvador): new data and discussion on the natural state of the system. *Per. Mineral., 75*, *2*, 293-312.

Sheppard, D., and Mroczek, E., 2004: Greenhouse gas emissions from the exploitation geothermal systems. *IGA Quaterly, 55*, 11-13.

SIGET, 2008: Electrical statistics, preliminary report: First semester 2008 (in Spanish),. SIGET, 104 pp.

Sinclair, A.J., 1974: Selection of threshold values in geochemical data using probability graph. *Journal of Geochemical Exploration, 3*, 129-149.

Sorey, M.L., Evans, W.C., Kennedy, B.M., Farrar, C.D., Hainsworth, L.J., and Hausback, B., 1998: Carbon dioxide and helium emissions from a reservoir of magmatic gas beneath Mammoth Mountain, California. *J. Geophys. Res., 103*, *15*, 303-323.

Tonani, F., and Miele, G., 1991: Methods for measuring flow of carbon dioxide through soils in the volcanic setting. *Proceedings of the International Conference on Active Volcanoes and Risk Mitigation,* 27 August-1 September, 1991, Napoli, Italy (abstract).

Van Loon, G.W., and Duffy, S.J., 2005: *Environmental chemistr,y a global perspective* (2^{nd} edition). Oxford University Press Inc., NY, 532 pp.

Wiese, F., Fridriksson, Th., and Ármannsson, H., 2008: *CO_2 fixation by calcite in high-temperature geothermal systems in Iceland.* Report prepared for Rannís, Hitaveita Sudurnesja hf., Orkuveita Reykjavíkur, Landsvirkjun and Orkustofnun, 35 pp.

Wolff-Boenisch, D., Gislason S.R., Oelkers E.H., and Putnis C.V., 2004: The dissolution rates of natural glasses as a function of their composition at pH 4 and 10.6, and temperatures from 25 to 74°C. *Geochim. Cosmochim. Acta, 68, 23,* 4843-4858.

Wolff-Boenisch, D., Gislason S.R., and Oelkers E.H., 2006: The effect of crystallinity on dissolution rates and CO_2 consumption capacity of silicates. *Geochim. Cosmochim. Acta, 70,* 858-870.

APPENDIX 1: Chemical analyses of fluids from the wells studied

TABLE 1a: Chemical analyses of the fluids from the two-phase discharging wells

WELL	Sampling Date	Na	K	Ca	Mg	Cl (mg/kg)	SO4	CO2	SiO2	B	pH/20°C	CO2 in steam*	Sampling Pressure[1]	Aquifer T (°C)[2]	Discharged Enthalpy[3]
TR-17	16/11/06	3907	807.5	288.4	0.149	7372	21.4	3.78	702.6	143.6	6.5	77.64	6.40	253	1100
	21/05/07	4692	882.9	187.9	0.247	8400	9.7	2.22	821.7	161.6	6.22	77.02	7.00	253	1185
	23/01/08	4643	901.4	184.0	0.189	8527	7.2	7.03	795.9	169.4	6.26	76.24	8.00	253	1193
	13/01/09	4831	827	194.2	0.160	8430	11.5	2.28	799.8	160.1	6.18	79.37	8.60	253	1199
TR-17 A	28/08/07	4329	705.5	255.4	0.174	7719	17.7	3.57	627.0	134.2	6.88	54.09	7.62	279	1161
	27/09/07	4155	679.5	249.9	0.216	7698	26.2	4.49	499.7	134.0	6.88	54.46	7.8	279	1167
	23/01/08	4143	690.4	247.1	0.265	7648	23.6	2.75	523.2	150.0	6.92	55.56	7.68	279	1100
	31/03/08	4238	670.3	307.6	0.301	7698	26.3	3.72	539.7	122.9	6.98	56.25	7.8	279	1138
TR-17 B	08/12/06	3653	680.3	172.6	0.214	6619	26.8	5.69	650.7	115.4	6.78	84.46	6.95	266	1194
	24/01/07	3808	645.8	206.0	0.188	6831	20.6	9.83	646.0	120.8	6.94	101.45	6.87	266	1095
	18/02/08	3864	676.3	207.2	0.177	7022	21.5	8.97	623.6	170.8	6.71	97.05	8.00	266	1146
	13/01/09	4054	683.9	206.2	0.180	7295	17.9	3.77	651.5	150.9	6.56	91.70	8.10	266	1209
TR-18	17/09/07	2067	306.1	43.6	0.010	3575	28.2	15.09	588.7	90.7	7.53	121.33	8.04	261	1205
	31/03/08	1989	323.5	52.5	0.010	3505	23.5	13.65	628.6	74.6	7.57	131.57	7.85	261	1168
	27/05/08	2072	318.3	42.3	0.010	3556	19.7	6.92	582.3	80.3	7.56	132.23	7.85	261	1169
	12/08/08	2043	321.3	42.1	0.010	3549	29.3	15.80	590.1	87.8	7.60	130.40	7.56	261	1137

* in mmol/100 mol steam

[1] in bar-g

[2] Measured

[3] in (kJ/kg)

TABLE 1b: Calculated chemical composition in selected geothermal wells

WELL	Sampling Date	Na	K	Ca	Mg	Cl	SO4	CO2	SiO2	B
						(mg/kg)				
TR-17	16/11/06	3022	624.6	223.1	0.115	5702	16.6	432.6	543.4	111.1
	21/05/07	3472	653.4	139.1	0.183	6216	7.2	490.7	608.1	119.6
	23/01/08	3500	679.5	138.7	0.142	6428	5.4	463.9	600.0	127.7
	13/01/09	3651	625.0	146.8	0.121	6371	8.7	474.9	604.4	121.0
TR-17 A	28/08/07	3490	568.7	205.9	0.140	6222	14.3	259.1	505.4	108.2
	27/09/07	3536	578.2	212.7	0.184	6551	22.3	202.9	425.2	114.0
	23/01/08	3488	581.2	208.0	0.223	6438	19.9	217.0	440.4	126.3
	31/03/08	3547	561.0	257.4	0.252	6442	22.0	227.2	451.7	102.9
TR-17 B	08/12/06	2900	540.1	137.0	0.169	5255	21.3	429.9	516.6	91.6
	24/01/07	3027	513.3	163.7	0.149	5430	16.4	431.1	513.5	96.0
	18/02/08	3129	547.6	167.8	0.143	5686	17.4	458.3	505.0	138.3
	13/01/09	3248	547.9	165.2	0.144	5844	14.3	448.6	521.9	120.9
TR-18	17/09/07	1699	251.6	35.8	0.008	2938	23.2	540.4	483.8	74.5
	31/03/08	1606	261.2	42.4	0.008	2829	18.9	630.5	507.4	60.2
	27/05/08	1705	161.9	34.8	0.008	2926	16.2	578.4	479.1	66.1
	12/08/08	1672	262.9	34.5	0.008	2904	24.0	592.1	482.8	71.8

APPENDIX 2: Saturation index for well studied

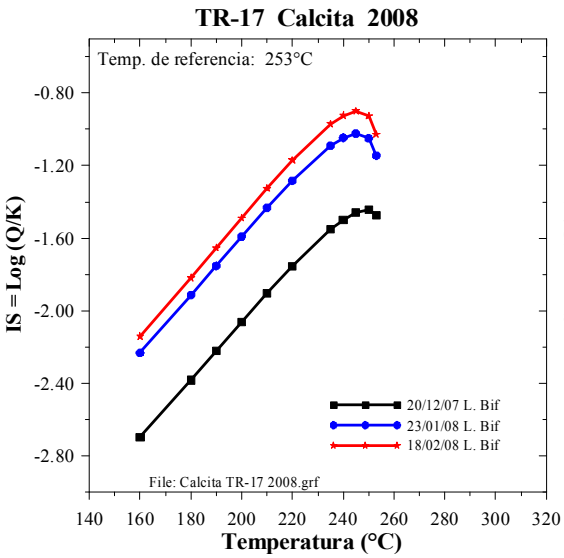

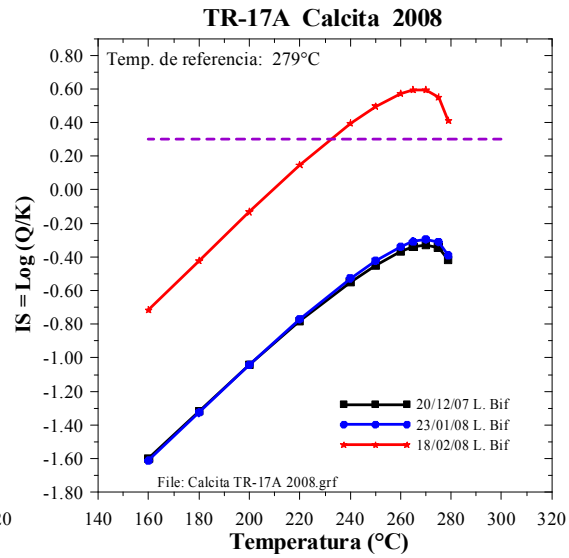

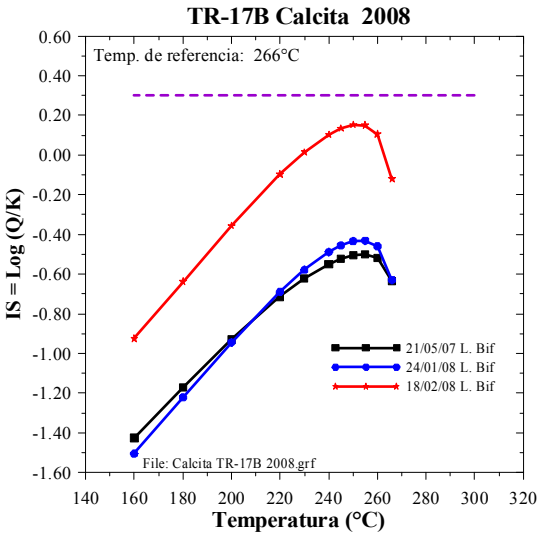

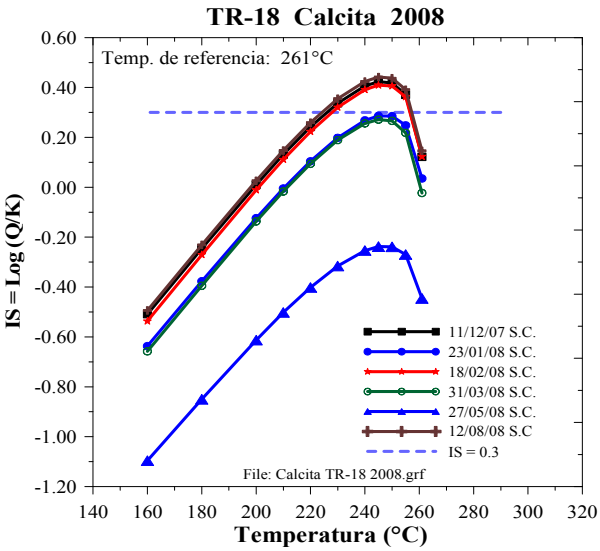

APPENDIX 3: Operational characteristics of the Berlin power plant period 2007-2008

TABLE 1a: Operation characteristics of the Berlin power plant in the year 2007. Mass of steam (1 x 10^3 t), produced power in GWh and steam flow rate for power production of 1 MWe

2007	U1	U2	U3	U1	U2	U3	U4	kg /Mwe-s		
	Steam kilotones			Gross generation (GWh)				U1	U2	U3
January	132.578	136.100	201.730	20.232	20.101	8.917		1.820	1.881	6.284
February	119.856	123.030	235.513	18.272	18.127	26.871		1.822	1.885	2.435
March	129.396	134.664	251.438	19.895	19.748	24.017		1.807	1.894	2.908
April	129.727	134.875	257.271	19.579	19.428	23.333		1.840	1.928	3.063
May	134.784	137.864	293.021	20.201	20.049	30.768		1.853	1.910	2.645
Jun	131.095	134.736	280.467	19.724	19.563	26.119		1.846	1.913	2.983
July	134.079	139.848	259.007	20.117	20.230	25.973		1.851	1.920	2.770
August	135.050	138.684	225.955	20.208	20.047	25.658		1.856	1.922	2.446
September	131.510	55.638	264.763	19.751	8.114	30.753		1.850	1.905	2.392
October	134.441	136.498	85.365	20.161	20.145	9.771		1.852	1.882	2.427
November	127.300	132.102	0.000	19.184	19.401	0.000	2.022	1.843	1.891	0.000
December	133.013	134.221	237.864	20.102	19.860	25.755	2.243	1.838	1.877	2.565
Total	**1572.830**	**1538.261**	**2592.393**	**237.425**	**224.815**	**257.936**	**4.265**	**1.840**	**1.901**	**2.792**

TABLE 1b: Operational characteristics of the Berlin power plant in the year 2008. Mass of steam (1 x10^3 t), produced power in GWh and steam flow rate for power production of 1 MWe

2008	U1	U2	U3	U1	U2	U3	U4	kg /Mwe-s		
	Steam kilotones			Gross generation (GWh)				U1	U2	U3
January	133.546	134.564	271.847	20.152	20.046	31.679		1.841	1.865	2.384
February	125.566	127.193	233.541	18.856	18.894	24.344		1.850	1.870	2.665
March	134.926	135.855	271.502	20.155	20.176	32.132		1.860	1.870	2.347
April	129.356	130.318	256.005	19.130	19.154	29.852		1.878	1.890	2.382
May	136.125	137.420	259.330	20.088	20.197	29.595		1.882	1.890	2.434
Jun	131.288	133.290	175.656	19.406	19.417	18.578	2.727	1.879	1.907	2.626
July	136.063	138.740	275.280	20.186	20.228	30.489	0.793	1.872	1.905	2.508
August	134.988	140.760	253.796	19.991	20.039	28.789	1.604	1.876	1.951	2.449
September	69.689	133.990	210.545	10.382	18.615	24.887	3.555	1.865	1.999	2.350
October	131.099	143.149	206.015	19.927	19.922	21.750	2.791	1.828	1.996	2.631
November	126.781	134.988	201.690	19.375	19.454	19.566		1.818	1.927	2.863
December	131.671	138.009	260.666	19.879	20.032	29.807	4.727	1.840	1.914	2.429
Total	**1521.098**	**1628.274**	**2875.876**	**227.525**	**236.173**	**321.469**	**16.195**	**1.857**	**1.915**	**2.485**

APPENDIX 4: Locations and CO_2 fluxes in g m^{-2} d^{-1}

TABLE 1a: CO_2 flux in g m^{-2} d^{-1}

ID	DATE	COORDINATES		Log CO2 FLUX (g/m^{-2} d^{-1})
		X	Y	
L1-01	3/11/2008	555008	265996	1.29
L1-02	3/11/2008	554756	266010	0.50
L1-03	3/11/2008	554501	266015	0.96
L1-04	3/11/2008	554253	266010	0.81
L1-05	3/11/2008	553992	265989	0.79
L1-06	3/11/2008	553762	266021	0.99
L1-07	3/13/2008	553524	265996	0.69
L1-08	3/13/2008	553252	265998	1.43
L1-09	3/11/2008	553003	266005	1.20
L1-10	3/10/2008	552765	265981	0.74
L1-11	3/10/2008	552493	266000	0.75
L1-12	3/10/2008	552246	266006	0.66
L1-13	3/10/2008	551986	266007	0.75
L1-14	3/25/2008	551753	266003	1.11
L1-15	3/25/2008	551495	266006	0.77
L1-16	3/25/2008	551243	266002	1.29
L1-17	3/25/2008	551000	265993	0.79
L2-01	3/12/2008	554976	265725	0.52
L2-02	3/12/2008	554735	265742	1.16
L2-03	3/12/2008	554498	265739	1.44
L2-04	3/11/2008	554242	265755	0.92
L2-05	3/26/2008	554004	265740	1.09
L2-06	3/26/2008	553742	265752	0.85
L2-07	3/13/2008	553504	265740	1.36
L2-08	3/14/2008	553253	265752	1.17
L2-09	3/13/2008	553013	265772	0.97
L2-10	3/25/2008	552752	265753	0.09
L2-11	3/25/2008	552490	265755	1.32
L2-12	3/25/2008	552250	265751	0.82
L2-15	3/25/2008	551504	265741	0.94
L2-16	3/25/2008	551255	265750	0.69
L2-17	3/26/2008	550989	265742	0.89
L3-01	3/12/2008	555018	265521	1.06
L3-02	4/4/2008	554758	265524	0.94
L3-03	4/8/2008	554515	265498	1.48
L3-04	3/12/2008	554255	265500	0.92
L3-05	3/14/2008	553978	265500	0.85
L3-06	3/14/2008	553745	265501	1.36
L3-07	3/14/2008	553511	265504	0.53
L3-08	3/13/2008	553257	265498	1.15
L3-09	3/11/2008	553013	265494	0.44
L3-10	3/11/2008	552742	265506	0.81
L3-11	3/11/2008	552506	265496	1.09
L3-12	3/25/2008	552242	265483	0.47
L3-13	3/6/2008	551933	265746	0.88
L3-16	3/25/2008	551260	265510	0.52
L3-17	3/26/2008	550995	265522	1.01
L4-01	3/12/2008	554999	265246	0.64
L4-02	4/8/2008	554738	265251	0.89
L4-03	4/4/2008	554491	265256	1.08

TABLE 1b: CO_2 flux in g m^{-2} d^{-1}

ID	DATE	COORDINATES		Log CO2 FLUX (g/m^{-2} d^{-1})
		X	Y	
L4-07	3/26/2008	553514	265247	0.75
L4-08	3/13/2008	553248	265252	0.97
L4-09	3/13/2008	553022	265253	0.59
L4-10	3/13/2008	552762	265260	0.93
L4-11	3/26/2008	552506	265254	0.83
L4-12	2/28/2008	552214	265173	0.78
L4-14	3/4/2008	551750	265250	0.66
L4-15	3/5/2008	551513	265253	0.30
L4-16	3/7/2008	551250	265250	0.12
L4-17	3/25/2008	550990	265245	1.08
L5-01	3/12/2008	554993	264997	0.74
L5-02	4/8/2008	554742	265003	1.00
L5-03	4/4/2008	554491	265006	1.49
L5-09	3/13/2008	552996	265009	0.79
L5-10	3/13/2008	552721	265029	0.94
L5-11	3/13/2008	552560	265046	1.14
L5-12	2/13/2008	552356	265000	0.71
L5-13	2/27/2008	552000	265000	1.06
L5-14	3/3/2008	551750	265000	0.59
L5-15	3/4/2008	551544	265008	0.21
L5-16	3/25/2008	551250	265012	1.05
L5-17	3/25/2008	550974	264998	1.04
L6-01	3/12/2008	555004	264748	1.20
L6-02	4/4/2008	554731	264752	1.31
L6-03	4/8/2008	554994	264754	1.36
L6-04	4/10/2008	554250	264762	1.67
L6-06	4/10/2008	553721	264754	1.53
L6-07	4/10/2008	553507	264764	0.90
L6-08	4/10/2008	553274	264735	1.45
L6-09	4/10/2008	553079	264830	1.10
L6-10	4/10/2008	552754	264769	1.55
L6-11	3/5/2008	552500	265250	0.30
L6-12	2/28/2008	552250	265250	0.34
L6-13	3/5/2008	552000	265250	0.40
L6-14	3/5/2008	551791	265201	1.12
L6-15	3/5/2008	551500	265250	0.32
L6-16	3/25/2008	551250	264762	0.59
L6-17	3/26/2008	550997	264761	0.76
L7-01	3/12/2008	555001	264484	1.04
L7-02	3/12/2008	554752	264498	1.33
L7-03	4/3/2008	554505	264501	1.25
L7-04	4/3/2008	554241	264506	0.97
L7-05	4/3/2008	554000	264514	1.57
L7-10	2/26/2008	552700	264500	0.80
L7-11	2/19/2008	552488	264535	0.41
L7-12	2/19/2008	552250	264500	0.43
L7-13	2/13/2008	552000	264500	0.31
L7-14	2/14/2008	551750	264500	0.80
L7-15	2/14/2008	551500	264500	-0.23
L8-01	3/12/2008	554997	264235	1.22

TABLE 1c: CO_2 flux in g m^{-2} d^{-1}

ID	DATE	COORDINATES		Log CO2 FLUX (g/m^{-2} d^{-1})
		X	Y	
L8-03	4/3/2008	554506	264282	1.68
L8-04	4/3/2008	554249	264256	1.31
L8-05	4/3/2008	553996	264257	1.62
L8-06	4/8/2008	553733	264249	1.39
L8-10	2/26/2008	552758	264239	0.54
L8-11	2/26/2008	552554	264262	0.51
L8-12	2/20/2008	552250	264250	0.95
L8-13	2/20/2008	552000	264250	0.84
L8-14	3/26/2008	551734	264255	0.75
L8-15	3/27/2008	551509	264254	0.27
L9-01	4/7/2008	555007	263891	1.75
L9-02	4/7/2008	554754	263960	1.01
L9-03	4/7/2008	554502	263974	1.06
L9-05	4/2/2008	554014	264039	3.05
L9-06	3/31/2008	553740	264000	1.13
L9-07	3/31/2008	553500	264004	1.59
L9-08	3/31/2008	553242	264005	1.18
L9-11	2/26/2008	552510	264081	0.23
L9-12	2/21/2008	552250	264000	0.40
L9-13	2/20/2008	552086	264070	1.88
L9-14	4/1/2008	551750	263993	0.92
L9-15	3/27/2008	551496	263999	0.94
L10-01	4/8/2008	555018	263756	1.63
L10-03	4/7/2008	554497	263741	2.69
L10-04	4/7/2008	554258	263726	1.13
L10-05	4/2/2008	553895	263800	1.74
L10-06	3/31/2008	553758	263739	0.95
L10-07	4/2/2008	553512	263736	1.95
L10-08	3/28/2008	553262	263747	1.04
L10-09	3/28/2008	553005	263750	0.25
L10-10	3/28/2008	552766	263761	1.01
L10-11	3/27/2008	552497	263741	0.67
L10-12	2/25/2008	552258	263765	0.47
L10-13	4/1/2008	551999	263745	0.77
L10-14	4/1/2008	551745	263752	1.22
L10-15	3/27/2008	551497	263758	0.50
L11-01	4/8/2008	555018	263618	0.82
L11-03	4/7/2008	554495	263582	0.97
L11-04	4/7/2008	554293	263556	1.53
L11-05	4/2/2008	554005	263557	0.88
L11-06	4/2/2008	553773	263499	0.99
L11-07	4/2/2008	553507	263500	0.94
L11-08	3/28/2008	553246	263500	0.69
L11-09	3/28/2008	552994	263500	0.83
L11-10	4/1/2008	552689	263525	2.77
L11-11	4/1/2008	552502	263510	0.97
L11-12	3/27/2008	552263	263479	1.04
L11-13	3/27/2008	551990	263522	0.32
L11-14	3/27/2008	551755	263504	1.65
L11-15	3/27/2008	551492	263503	0.69

APPENDIX 5: Results of total carbon measurements and computed captured CO_2

TABLE 1: Well TR-17 borehole length, vertical depth (TVD) and elevation in m, Northings and Eastings in Lambert coordinates, measured carbon in % weight and computed CO_2 in kg/m^3

WELL	Borehole Length (m)	Vertical Depth (m) TVD	X	Y	Z (m a.s.l.)	Carbon C (% wt)	Captured CO_2 (kg/m³)
TR-17	0	0	553497	265243	1080		
	320	320	553497	265243	760	0.08	**8.63**
	410	410	553497	265243	670	0.87	**89.22**
	600	600	553497	265243	480	1.45	**148.94**
	820	820	553497	265243	260	1.14	**116.96**
	1000	1000	553497	265243	80	0.30	**30.96**
	1200	1200	553497	265243	-120	0.13	**12.87**
	1395	1395	553497	265243	-315	0.38	**39.21**
	1500	1500	553497	265243	-420	0.01	**1.39**
	2000	2000	553497	265243	-920	0.01	**0.82**
	2417	2417	553497	265243	-1337	0.01	**0.54**

TABLE 2: Well TR-17A borehole length, vertical depth (TVD) and elevation in m, Northings and Eastings in Lambert coordinates, measured carbon as % weight and computed CO_2 in kg/m^3

WELL	Borehole Length (m)	Vertical Depth (m) TVD	X	Y	Z (m a.s.l.)	Carbon C (% wt)	Captured CO_2 (kg/m³)
TR-17A	**0**	**0**	553489	265234	1080		
	100	99.99	553489	265236	980	0.00	**0.00**
	250	249.97	553489	265243	830	1.89	**193.99**
	500	499.84	553489	265269	580	0.56	**57.78**
	780	779.32	553493	265317	301	0.08	**8.10**
	1055	1053.88	553507	265366	26	1.31	**134.10**
	1200	1198.46	553515	265598	-118	0.27	**27.89**
	1780	1727.76	553667	267579	-648	0.11	**11.50**
	2110	2012.68	553780	269667	-933	0.04	**4.41**
	2457	2320.80	553876	272409	-1241	0.05	**5.53**
	2628	2474.44	553920	273381	-1394	0.00	**0.21**

TABLE 3: Well TR-17B borehole length, vertical depth (TVD) and elevation in m, Northings and Eastings in Lambert coordinates, measured carbon as % weight and computed CO_2 in kg/m^3

WELL	Borehole Length (m)	Vertical Depth (m) TVD	X	Y	Z (m a.s.l.)	Carbon C (% wt)	Captured CO_2 (kg/m³)
TR-17B	0	0	553493	265239	1074		
	160	160.00	553493	265240	914	0.02	**1.72**
	315	314.96	553493	265245	759	1.36	**139.57**
	410	409.91	553493	265259	664	0.69	**71.10**
	500	499.85	553496	265266	574	0.42	**43.31**
	600	599.76	553499	265271	474	0.68	**69.41**
	700	699.64	553496	265273	374	0.30	**30.31**
	845	844.57	553493	265278	229	0.04	**3.77**
	1100	1099.51	553498	265294	-26	1.10	**113.00**
	1150	1149.46	553500	265313	-76	0.89	**91.64**
	1250	1248.52	553513	265357	-175	0.01	**0.70**

TABLE 4: Well TR-18, borehole length, vertical depth (TVD) and elevation in m, Northings and Eastings in Lambert coordinates, measured carbon as % weight and computed CO_2 in kg/m^3

WELL	Borehole Length (m)	Vertical Depth (m) TVD	X	Y	Z (m a.s.l.)	Carbon C (% wt)	Captured CO_2 (kg/m³)
TR-18	0	0	552149	264716	995		
	250	250	552149	264716	745	0.09	**9.14**
	480	480	552149	264716	515	0.36	**36.84**
	750	750	552149	264716	245	0.54	**55.41**
	995	995	552149	264716	0	0.53	**54.60**
	1205	1205	552149	264716	-210	1.03	**105.45**
	1290	1290	552149	264716	-295	0.50	**51.34**
	1400	1400	552149	264716	-405	0.58	**59.38**
	1845	1845	552149	264716	-850	0.61	**62.60**
	2600	2600	552149	264716	-1605	0.01	**1.24**

TABLE 5: Well TR-18A, borehole length, vertical depth (TVD) and elevation in m, Northings and Eastings in Lambert coordinates, measured carbon in % weight and computed CO_2 in kg/m^3

WELL	Borehole Length (m)	Vertical Depth (m) TVD	X	Y	Z (m a.s.l.)	Carbon C (% wt)	Captured CO_2 (kg/m³)
TR-18A	0	0	552151	264721	995		
	100	99.99	552151	264722	895	0.06	**5.98**
	200	199.98	552151	264725	795	0.06	**6.18**
	245	244.97	552151	264731	750	0.09	**9.63**
	340	339.93	552151	264738	655	0.06	**6.06**
	520	519.81	552151	264751	475	0.58	**59.24**
	605	604.70	552152	264781	390	0.42	**43.08**
	680	679.38	552156	264881	316	0.51	**51.92**
	735	733.75	552164	264972	261	0.64	**65.35**
	800	798.07	552173	265098	197	0.76	**77.86**
	900	896.64	552189	265205	98	0.11	**11.01**